HHS Public Access

Author manuscript

Cell Rep. Author manuscript; available in PMC 2022 August 25.

Published in final edited form as:

Cell Rep. 2022 January 11; 38(2): 110215. doi:10.1016/j.celrep.2021.110215.

Helminth resistance is mediated by differential activation of recruited monocyte-derived alveolar macrophages and arginine depletion

Fei Chen[1,2], **Darine W. El-Naccache**[1,2,8], **John J. Ponessa**[1,2,8], **Alexander Lemenze**[1,3], **Vanessa Espinosa**[1,4], **Wenhui Wu**[1,2], **Katherine Lothstein**[1,2], **Linhua Jin**[1,2], **Olivia Antao**[1,2], **Jason S. Weinstein**[1,2], **Payal Damani-Yokota**[5], **Kamal Khanna**[5,6], **Peter J. Murray**[7], **Amariliz Rivera**[1,4], **Mark C. Siracusa**[1,2,9,*], **William C. Gause**[1,2,9,10,*]

[1]Center for Immunity and Inflammation, New Jersey Medical School, Rutgers—The State University of New Jersey, Newark, NJ, USA

[2]Department of Medicine, New Jersey Medical School, Rutgers—The State University of New Jersey, Newark, NJ, USA

[3]Department of Pathology, Immunology, and Laboratory Medicine, New Jersey Medical School, Rutgers—The State University of New Jersey, Newark, NJ, USA

[4]Department of Pediatrics, New Jersey Medical School, Rutgers—The State University of New Jersey, Newark, NJ, USA

[5]Department of Microbiology, New York University Langone Health, New York, NY 10016, USA

[6]Perlmutter Cancer Center, New York University Langone Health, New York, NY 10016, USA

[7]Max Planck Institute of Biochemistry, Martinsried 82152, Germany

[8]These authors contributed equally

[9]These authors contributed equally

[10]Lead contact

SUMMARY

Macrophages are known to mediate anti-helminth responses, but it remains uncertain which subsets are involved or how macrophages actually kill helminths. Here, we show rapid monocyte recruitment to the lung after infection with the nematode parasite *Nippostrongylus brasiliensis*. In this inflamed tissue microenvironment, these monocytes differentiate into an alveolar macrophage

*Correspondence: mark.siracusa@njms.rutgers.edu (M.C.S.), gausewc@njms.rutgers.edu (W.C.G.).

AUTHOR CONTRIBUTIONS

Conceptualization, W.C.G., M.C.S., F.C., A.R., D.W.E.-N., P.J.M., and J.S.W.; methodology, F.C., D.W.E.-N., J.J.P., V.E., W.W., K.L., O.A., P.D.-Y., and K.K.; formal analysis, F.C., A.L., W.C.G., J.S.W., L.J., V.E., M.C.S., and J.J.P.; investigation, all authors; writing – original draft, W.C.G., F.C., and M.C.S; writing – review & editing, all authors; funding acquisition, W.C.G., M.C.S., J.J.P., D.W.E.-N., and K.K.

SUPPLEMENTAL INFORMATION

Supplemental information can be found online at https://doi.org/10.1016/j.celrep.2021.110215.

DECLARATION OF INTERESTS

M.C.S. is the founder and President of NemaGen Discoveries.

(AM)-like phenotype, expressing both SiglecF and CD11c, surround invading parasitic larvae, and preferentially kill parasites *in vitro*. Monocyte-derived AMs (Mo-AMs) express type 2-associated markers and show a distinct remodeling of the chromatin landscape relative to tissue-derived AMs (TD-AMs). In particular, they express high amounts of arginase-1 (Arg1), which we demonstrate mediates helminth killing through L-arginine depletion. These studies indicate that recruited monocytes are selectively programmed in the pulmonary environment to express AM markers and an anti-helminth phenotype.

Graphical abstract

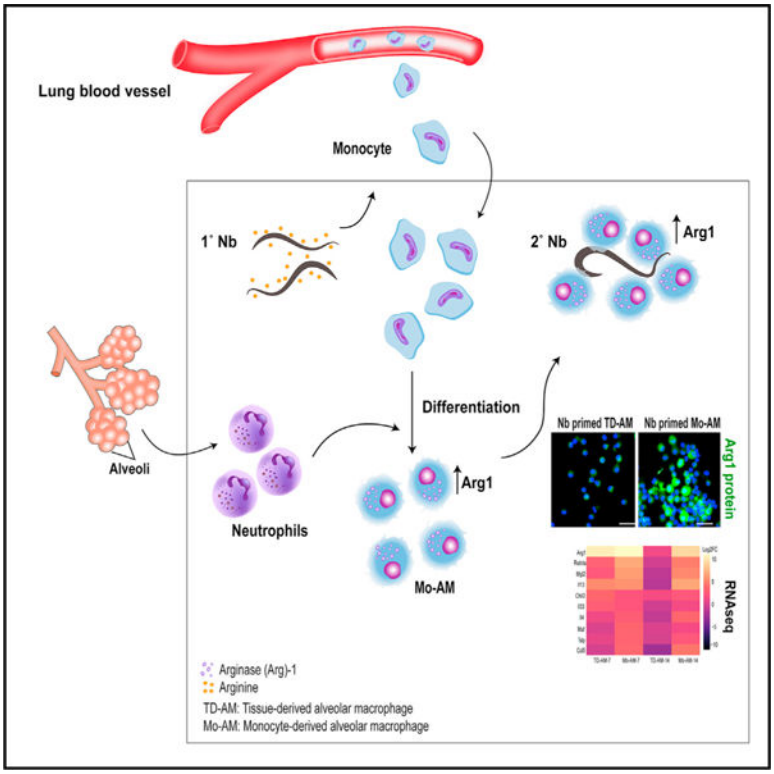

In brief

Chen et al. show that, during helminth infection, monocytes recruited to the lung can assume an alveolar-like macrophage phenotype and differentially express markers associated with tissue remodeling and allergic inflammation, including arginase-1 (Arg1). Arg1 mediates helminth killing through depletion of arginine, indicating nutrient deprivation as a host resistance mechanism.

INTRODUCTION

Helminth infections trigger potent type 2 immune responses characterized by elevations in interleukin (IL)-4, IL-5, and IL-13. This response mediates host protection through limiting the parasite burden and by mitigating tissue damage associated with the trafficking of these large multicellular parasites through host tissues (Gause et al., 2013). Although helminth

infections represent a major global health problem, effective vaccine strategies remain elusive, likely in part because the cellular and molecular mechanisms through which the anti-helminth immunity is mediated remain unclear. A critical stage of the life cycle of many helminths, including intestinal nematode parasites, involves transit through the host lung. Previous studies have indicated that the lung plays a significant role in early parasite clearance and, as such, is a potential target for therapeutic and vaccine strategies to promote host resistance (Chen et al., 2014; Harvie et al., 2010).

Both lymphoid and myeloid cells play important roles in promoting type 2 inflammation and anti-helminth immunity. For example, T cells, B cells, myeloid cells, and innate lymphoid type 2 cells are activated and promote robust levels of IL-4, IL-5, and IL-13 following a helminth challenge. Importantly, studies also indicate that macrophages and neutrophils contribute to host protection by directly killing parasitic larvae and initiating the healing of parasite-affected tissues (Bouchery et al., 2020; Chen et al., 2012, 2014; Sutherland et al., 2014). Neutrophils not only directly target helminths (Bouchery et al., 2020), but also stimulate macrophages to assume an alternatively activated state required for their anti-helminth effector functions (Bosurgi et al., 2017; Chen et al., 2014). Recent studies indicate that macrophages primed by helminths in the intestine, lung, and skin can mediate helminth killing both *in vitro* and in these tissue microenvironments (Anthony et al., 2006; Chen et al., 2014; Esser-von Bieren et al., 2013; Gause et al., 2020; Harvie et al., 2010; Obata-Ninomiya et al., 2013).

Tissue-resident macrophage populations can be subdivided into tissue-derived macrophages (TD-macs) and monocyte-derived macrophages (Mo-macs). TD-macs develop during the early stages of fetal development from the yolk sac and fetal liver and populate tissues under steady-state conditions, whereas Mo-macs develop from bone-marrow-resident precursor cells and can enter tissues in the context of inflammation (Bleriot et al., 2020; Gundra et al., 2014; Jenkins et al., 2011; Scott et al., 2014). In the lung microenvironment, TD alveolar macrophages (TD-AMs) mediate homeostasis through multiple mechanisms, including surfactant recycling, and also provide surveillance for the early recognition of pathogens invading the airways (Hussell and Bell, 2014). Other scarce TD interstitial macrophage populations can also have distinct properties (Ural et al., 2020). During infection, monocytes are rapidly recruited to the lung, where they can differentiate into macrophages. Recent studies suggest that monocytes can also differentiate into an AM-like phenotype and that these Mo-AMs can function differently than TD-AMs (Aegerter et al., 2020). In one study, the Mo-AMs were the predominate lung macrophage subset contributing to fibrosis in a bleomycin-induced lung injury model (Misharin et al., 2017). Despite these substantial advances in understanding macrophage ontogeny, studies examining the development of Mo-AMs have primarily relied on radiation chimeras or other non-physiological approaches, raising questions as to the physiological significance of these observations. Further, whether Mo-AMs populate the lung and perform distinct functions in the context of helminth infections remains to be determined.

Although the anti-helminth qualities of macrophages are well-documented, there is a substantial knowledge gap regarding the mechanisms they employ to promote parasite-killing. Previous studies have shown that arginase (Arg) activity (Chen et al., 2014; Kreider

et al., 2007; Obata-Ninomiya et al., 2013), specifically Arg1 (Esser-von Bieren et al., 2013), is required for the anti-helminth properties of macrophages. Arg1 is known to mediate a cascade of effects leading to potentially toxic urea production and also polyamine synthesis, which may contribute to immune cell activation and proliferation (Kreider et al., 2007). Arg1 can also mediate the localized depletion of arginine, which can have immunoregulatory effects on activated immune cells such as T cells (Pesce et al., 2009). However, whether any of these or other potentially associated mechanisms are important in regulating the macrophage-mediated killing of helminth parasites and whether they are distinctly initiated in specific subsets of macrophages remain uncertain.

Infection with the intestinal nematode parasite *N. brasiliensis* (Nb) is a well-established rodent model showing a similar life cycle to human hookworms. Use of this model has substantially advanced our understanding of inflammation and macrophage biology in lung damage and repair caused by transiting helminths. When infected with Nb, infective third-stage larvae (L3) migrate from the skin to the lung before entering the small intestine. In the lung, both innate and adaptive components of the type 2 immune response interact with the migrating parasitic larvae (Chen et al., 2012; Harvie et al., 2010; Sutherland et al., 2014). Previous studies have shown that CD4 T cell depletion at the time of secondary inoculation does not affect accelerated resistance, which is also intact in B cell-deficient mice (Katona et al., 1988; Liu et al., 2010). However, lung macrophages primed by primary Nb inoculation have been shown to play an important role in acquired resistance, and highly purified helminth-primed lung macrophages can effectively kill L3 *in vitro* (Chen et al., 2014). Collectively, these data suggest that lung macrophages, in part, play important roles in promoting acquired resistance to helminths following a primary challenge.

Here, we investigated the role of lung macrophage subsets of different progenitor origins in mediating acquired resistance to Nb. We further elucidate the role of neutrophils in driving their effector function and reveal how Mo-macs mediate resistance against helminths via Arg1-dependent mechanisms.

RESULTS

Nb L3 enter the lung as early as 12 h after subcutaneous inoculation. To examine how parasite migration through the lung affected numbers of monocytes and macrophages, these populations were analyzed via flow cytometric analysis on days 1, 7, and 14 after inoculation. Marked increases in the total number of macrophages ($F4/80^+$, $CD64^+$) were observed by day 7 after inoculation (Figure 1A), while monocytes ($F4/80^+$, $Ly6C^+$) were markedly increased within 24 h, consistent with their rapid recruitment, peaked at day 7, and had dropped markedly by day 14 (Figure 1B). AMs ($CD64^+$, $F4/80^+$, $SiglecF^+$, $CD11c^+$) were slightly elevated as early as day 1 but showed marked increases, more than doubling by day 7 (Figure 1C). Non-AMs (hereafter, referred to as NAVMs) ($CD64^+$, $F4/80^+$, $SiglecF^-$, $CD11c^{var}$) were also markedly elevated by day 7 after Nb inoculation (Figure 1D). In comparison, eosinophils, also associated with Nb infection, were not elevated until day 7 after inoculation and remained elevated at day 14 (Figure 1E). Collectively, these data demonstrate that Nb infection promotes substantial changes in lung monocyte and macrophage subset dynamics. Further, these data suggest that the early influx of monocytes

observed in the lung may help to support the overall increases in lung macrophage populations observed post-infection.

Our previous studies have shown that by day 7 after Nb inoculation, sort-purified lung macrophages can effectively kill infectious Nb larvae (L3) following *in vitro* culture. By day 7, Nb larvae have left the lungs and entered the small intestine. However, the primed macrophages in the lung persist as late as 45 days after the primary inoculation and can now mediate accelerated resistance in subsequent infections or when transferred to otherwise naive recipients (Chen et al., 2014). Our studies are thus focused on this persistent anti-helminth macrophage population. Importantly, these bulk macrophage populations are comprised of both AMs and NAVMs. However, whether these two macrophage subsets equally or preferentially contribute to parasite-killing remains unknown. To test this, at day 7 after Nb inoculation, lung-cell suspensions were prepared as previously described (Chen et al., 2014), and AMs and NAVMs were sort-purified. Individual macrophage subsets (1×10^6/ml) were then cultured with exsheathed L3 (100/well) in 24-well plates for 5 days, as was previously done with bulk macrophages (Chen et al., 2014). As shown in Figure 2A, AMs were approximately 5 times more effective at killing L3 than were NAVMs. Assessment of parasite metabolic activity by assaying their ATP amounts (Chen et al., 2014) further showed significantly decreased activity in cultures seeded with AMs compared with those seeded with NAVMs (Figure 2B). Previous studies have shown that Arg1 production by macrophages is essential for the effective killing of parasitic larvae both *in vitro* and *in vivo* (Chen et al., 2012; Obata-Ninomiya et al., 2013). Therefore, to investigate whether the macrophage killing observed correlated with Arg1 production, AMs and NAVMs were assessed for cytoplasmic Arg1 expression at 7 days after Nb infection. As shown in Figure 2C, more than 10% of AMs expressed Arg1 after infection, while less than 3% of NAVMs from treated mice expressed Arg1, consistent with NAVMs being less effective in killing L3. Furthermore, the total number of Arg1-expressing AMs was significantly greater post-infection, while the numbers of Arg1-expressing NAVMs remained unchanged (Figure 2D). Collectively, these studies indicate that AMs mediate the majority of the parasite-killing capacity within lung macrophage compartments and that elevated cytoplasmic Arg1 protein expression is associated with that enhanced capacity in a subset representing ~10% of the total AM compartment.

Our previous studies showed that the transfer of bulk lung macrophages from Nb-primed mice into otherwise naive recipients was sufficient to mediate accelerated resistance, similar to the memory response observed after secondary challenge (Chen et al., 2014). To examine whether AMs also showed preferential resistance *in vivo*, AMs and NAVMs were sort-purified from the lungs of donor mice at day 7 after Nb inoculation and transferred to naive recipient mice, which were then inoculated with Nb. Unexpectedly, as shown in Figure 3A, both AMs and NAVMs were equally effective at mediating accelerated acquired resistance in recipient mice at 5 days after Nb inoculation. Given that the NAVMs expressed low Arg1 relative to the AMs, this raised the possibility that the transferred NAVMs were differentiating into an AM-like subset that acquired the ability to preferentially upregulate Arg1 and kill invading parasitic larvae. To test whether NAVMs could develop an AM-like phenotype in the lung, we isolated AMs and NAVMs from CD45.1 donor mice at day 7 after Nb inoculation and transferred these subsets intratracheally to naive congenic CD45.2

recipients. Recipient mice were rested for 2 days and inoculated with Nb, and 5 days later, lung-cell suspensions were collected and assessed for donor and recipient AM populations. As shown in Figure 3B, transferred CD45.1 donor NAVMs gave rise to a substantial number of macrophages with an AM-like phenotype ($CD45.1^+$, $CD64^+$, $F4/80^+$, $SiglecF^+$, $CD11c^+$) that represented ~10% of the total AM population in the CD45.2 congenic recipients. These data suggest that Mo-macs contained within the NAVM compartment may possess the capacity to acquire an AM-like phenotype. To further investigate the contribution of monocytes to the AM compartment post-Nb inoculation, we obtained CCR2 GFP reporter and CCR2 diphtheria toxin receptor (DTR) depleter mice. As early as day 1 after Nb inoculation, $CCR2^+$ monocytes were increased several folds in the lung, and these high levels were sustained as late as day 7 after Nb inoculation (Figure 3C). These data further support our findings presented in Figure 1B and highlight the significant recruitment of monocytes into the lung shortly after Nb inoculation. To further examine the extent to which monocytes contributed to the overall lung macrophage population after infection, $CCR2^{DTR}$ mice were inoculated with Nb and administered DT at −1, +1, and +3 days post-infection to deplete monocytes and Mo-macs. As expected, NAVMs were significantly reduced on day 7 post-infection after DT administration (Figure 3D), further corroborating a substantial contribution of monocytes to the NAVM compartment. However, intriguingly, AMs also showed a marked reduction in their expansion typically observed after Nb inoculation (Figure 3E). These data are consistent with a role for monocyte-derived cells contributing to the population expansion of AMs post-infection (Figure 3E). To confirm the selective depletion of DT treatment on $CCR2^+$ Mo-macs post-DT treatment, a separate myeloid population, eosinophils, which are $CCR2^-$, were also assessed. Eosinophils were also increased in the lung at 5 days after inoculation but were not affected by DT administration, consistent with the specificity of the treatment (Figure 3F). In aggregate, these data suggest that lung-infiltrating monocytes can acquire a tissue-resident AM phenotype and contribute substantially to the increased AM population observed post-infection. However, the contributions of these monocyte-derived AMs to host protection remained unknown.

To further explore the characteristics and functional significance of monocyte-derived AMs (Mo-AMs), we employed established fate-mapper mice that allow monocyte-derived cells in adult mice to be identified by their history of *Cx3cr1* expression (Gundra et al., 2017). With this mouse model, monocytes can be tracked in $Cx3cr1^{CreERT2\text{-}IRES\text{-}YFP}$ mice (abbreviated as $Cx3cr1^{Cre}$ mice), which express a tamoxifen (TAM)-inducible Cre recombinase (CreERT2) under the control of the endogenous promoter, followed by an internal ribosome entry site (IRES)–enhanced yellow fluorescent protein (EYFP) element (Gundra et al., 2017; Parkhurst et al., 2013).

To track the fate of the $CX3CR1^+$ monocytes, $Cx3cr1^{Cre}$ mice were crossed with $Rosa26^{stop\text{-}tdTomato}$ reporter mice (abbreviated as *R26*tdTomato mice), as previously described (Gundra et al., 2017). The resultant $Cx3cr1^{CreERT2\text{-}IRES\text{-}YFP/+}$ $Rosa26^{floxed\text{-}tdTomato/+}$ mice were inoculated with Nb and administered TAM at days −1 and +1 post-infection, which irreversibly labels $CX3CR1^+$ cells and their progeny by inducing the expression of tdTomato. As a control, naive $Cx3cr1^{CreERT2\text{-}IRES\text{-}YFP/+}$ $Rosa26^{floxed\text{-}tdTomato/+}$ mice were also administered TAM (Figure 4A). At day 7 after inoculation, lung-cell suspensions were collected and stained for markers

associated with conventional AMs (CD64$^+$, F4/80$^+$, SiglecF$^+$, CD11c$^+$) (Figures 4B and 4C). The gated AM subset was then analyzed for tdTomato expression. As shown in Figure 4D, ~30% of AMs were tdTomato$^+$ post-Nb infection, indicating that these cells were derived from CX3CR1$^+$ monocytes, while AMs from naive controls similarly treated with TAM showed <1% tdTomato expression (Figures S1A and S1B). Interestingly, tdTomato$^+$ cells persisted for up to a month post-infection (Figure 4E) and appeared phenotypically distinct from tdTomato$^-$ AMs by ultrastructural analysis (Figure 4F). Importantly, the use of these fate-mapping mice obviated the need for cell transfers and/or generation of chimeras for tracing the development of Mo-AMs, providing a useful, more physiological method for tracking and isolating Mo-AMs and TD-AMs. Next, we sort-purified TD-AMs (tdTomato$^-$) and Mo-AMs (tdTomato$^+$) at day 7 after Nb inoculation and cultured them with Nb L3 to test whether they possessed common or unique anti-helminth effector activity. Importantly, tdTomato$^+$ AMs derived from CX3CR1$^+$ monocytes were significantly more effective at impairing L3 metabolic activity (quantified by decreased ATP) and killing Nb larvae than their TD counterparts (Figures 4G and 4H). These studies thus indicate that after Nb inoculation, monocytes enter the lung and transition to an AM-like phenotype by acquiring expressions of SiglecF and CD11c. However, these data also suggest that Mo-AMs entering the lung post-infection are functionally distinct cells that preferentially damage and kill invading helminth larvae.

To examine the localization of Mo-AMs in lung tissue during Nb infection, *Cx3cr1*$^{\text{CreERT2-IRES-YFP/+}}$*Rosa26*$^{\text{floxed-tdTomato/+}}$ mice were administered TAM as described above and inoculated with Nb or left untreated. Bronchioalveolar lavage (BAL) was collected at day 7 after Nb inoculation. As shown in Figure S1C, Mo-AMs were not detected in the BAL of uninfected mice but were readily detectable in the BAL after Nb inoculation. In contrast, TD-AMs were readily detectable in the BAL of untreated and Nb-inoculated mice, with little change after infection (Figure S1D). Remaining lung tissue after collection of BAL was also assessed, and although Mo-AMs were not observed in uninfected mice as expected, Mo-AMs and TD-AMs were readily detectable after infection (Figures S1C and S1D). The presence of both AM subsets in the remaining lung tissue may be in part due to residual AMs in the alveoli and airways after lavage as well as a potential disruption of lung architecture resulting from infection. The *in situ* distribution of Mo-AMs was also assessed after the secondary inoculation. As shown in Figure S1E, marked increases in Mo-AMs in the BAL were detected after the secondary inoculation compared with those after the primary inoculation. Collectively, these data suggest that Mo-AMs have populated the lung and are ideally positioned to encounter invading parasitic larvae following a secondary challenge.

To visualize potential interactions between macrophages and larvae, the immunofluorescent stainings of cryosections from Cx3cr1$^{\text{CreERT2-IRES-YFP/+}}$*Rosa26*$^{\text{floxed-tdTomato/+}}$ mice were assessed after the Nb secondary inoculation. In these experiments, the second inoculation was administered 2 days after the first inoculation, and mice were sacrificed 6 days after the primary inoculation. This approach optimized visualization of trafficking parasites, as parasites are rapidly killed if the second inoculation is given at later time points and are thus not readily visualized. As shown in Figure 4I, using confocal microscopy, Mo-AMs (tdTomato$^+$, CD11c$^+$; yellow-orange) were observed immediately to be surrounding the

parasite after a second infection, whereas TD-AMs (tdTomato$^-$, CD11c$^+$; green) were more restricted to the airways. tdTomato$^+$, CD11c$^+$ cells (Mo-AMs) were also found in the airways, consistent with our flow cytometric analysis of BAL fluid. It should be noted that >98% of tdTomato$^+$, CD11c$^+$ cells exhibited an AM-like phenotype (F480$^+$, CD64$^+$, CD11c$^+$, SiglecF$^+$), as determined by flow cytometric analysis (Figures S1F and S1G).

Our findings that these Mo-AMs exhibit enhanced anti-helminth activity provokes the hypothesis that they are phenotypically distinct from their TD counterparts. To further test this, tdTomato$^+$ Mo-AMs and tdTomato$^-$ TD-AMs were sort-purified from TAM-treated fate-mapping mice at day 7 after Nb inoculation (as in Figure 4A) and were subjected to global transcriptome profiling. RNA sequencing (RNA-seq) analysis showed that Mo-AMs had a gene expression profie distinct from TD-AMs (Figure 5A). Even by day 14 post-infection, Mo-AMs maintained distinct profiles relative to TD-AMs and naive AMs, as determined by a pairwise Euclidean distance calculation (Figure 5A) and principal-components analysis (Figure 5B). Visualization of overall expression patterns by volcano plots showed more transcriptionally regulated genes in Mo-AMs compared with in TD-AMs at days 7 and 14 (Figure 5C). Venn diagrams of upregulated (Figure S2A) and downregulated (Figure S2B) genes further illustrated the distinct differences in expressed genes between Mo-AMs and TD-AMs after Nb inoculation. Ingenuity pathway analysis (IPA) further suggested that the TD- and Mo-AMs were functionally distinct (Figure S2C). Importantly, canonical type 2 pathways that are critical in mediating helminth resistance were more pronounced in Mo-AMs relative to TD-AMs (Figure 5D). Specifically, *Arg1*, *Retnla*, *Il-13*, and *Mgl2* were all increased in Mo-AMs relative to TD-AMs on day 7 and, to a lesser extent, on day 14 post-infection (Figure 5D). While Mo-AMs remained heightened in these responses on day 14 post-infection, TD-AMs had returned to baseline levels or, in some cases, below baseline levels by this time point (Figure 5D). These data suggest that Mo-AMs develop a potent M2-associated phenotype with anti-helminth functions. Additionally, wound-healing markers showed a similar pattern of increased expression in Mo-AMs (Figure S2D). Notably, peroxisome proliferator-activated receptor gamma (PPARg)-associated signaling pathways, important in lipid metabolism and surfactant homeostasis (Caputa et al., 2019), were instead significantly reduced in Mo-AMs relative to naive TD-AMs at days 7 (log2 fold change −1.72; FDR $p < 0.001$) and 14 ($\log_2$ fold change −1.95; FDR $p < 0.001$) after Nb inoculation. This may reflect a more prominent role for TD-AMs in homeostatic functions associated with lipid metabolism.

In independent experiments, we also employed transposase-accessible chromatin with sequencing (ATAC-seq) to examine changes in chromatin profiles by identifying transposase-accessible regulatory gene elements in both TD- and Mo-AMs subsets on day 7 post-infection. At a global level, the chromatin profiles of TD-AMs from Nb-inoculated mice were more similar to naive AMs than Mo-AMs from Nb-inoculated mice as indicated by an Euclidean distance calculation (Figure S3A) and principal-component analyses (Figure S3B). Differential volcano plot analyses revealed a greater accessibility of regulatory elements in the Mo-AMs from Nb-inoculated mice (Figure S3C), consistent with their increased overall transcription levels as observed with RNA-seq (Figures 5A–5D). A comparison of differentially called peaks in the four replicates of Mo-AMs versus TD-AMs identified 33,229 differentially expressed peaks (Figure S3D). No significant differences

were seen in chromatin accessibility for *Il33*. However, Mo-AMs had significant increases ($p < 0.001$) in chromatin accessibility at the *Arg1, Mgl2*, and *Retnla* promoter loci (Figure 5E). These findings suggest that the regulation of differential gene expression in TD-AMs is mediated at the level of chromatin accessibility. These data correlate with the increased *Arg1*, *Mgl2*, and *Retnla* transcripts also observed in the Mo-AMs (Figure 5D).

Analyses of *in vivo* proliferation of macrophage subsets showed similar levels of proliferation between TD-AMs and Mo-AMs at days 7 and 14 after inoculation (Figures S4A and S4B), consistent with both populations undergoing expansion in part through cell cycling. However, Seahorse real-time cell metabolic analyses using the mitochondria stress test revealed a higher oxygen consumption rate (OCR) and a higher extracellular acidification rate (ECAR), in Mo-AMs compared with TD-AMs at day 7 after inoculation (Figure S4C), indicating increased oxidative phosphorylation. We also observed increased *Il13* mRNA in both AM subsets after Nb inoculation. To corroborate these findings, we assessed IL-13 protein cytoplasmic staining and observed significant increases in IL-13 in AMs from Nb but in not *IL-4Ra*$^{-/-}$ mice at day 7 after inoculation (Figure S4D). These data are consistent with previous reports of lung macrophages producing IL-13 (Wu et al., 2015).

Collectively, our discovery-based studies revealed preferentially elevated levels of *Arg1* gene expression in Mo-AMs, which were also most effective at killing L3 (Figure 5D). To corroborate these findings, we performed qPCR on tdTomato^{+} Mo-AMs and tdTomato^{-} TD-AMs obtained from total lungs of *Cx3*cr1$^{\text{CreERT2-IRES-YFP/+}}$Rosa26$^{\text{floxed-tdTomato/+}}$ mice 8 days after L3 inoculation. As shown in Figure 6A, Arg1 mRNA was markedly elevated in tdTomato^{+} Mo-AMs relative to controls. To assess whether Arg1 protein was similarly increased in this subpopulation, Mo-AMs and TD-AMs were assayed for intracellular Arg1 protein expression by flow cytometric analysis. As shown in Figures 6B and 6C, Arg1 protein was expressed at considerably higher levels in fluorescence-activated cell sorting (FACS)-gated tdTomato^{+} Mo-AMs relative to tdTomato^{-} TD-AMs. We further corroborated these findings through cytology and immunofluorescent staining of AM subsets that showed preferential staining for Arg1 in Mo-AMs (Figure S5).

M2 macrophage activation is regulated by several factors including the production of type 2 cytokines by specialized innate immune cells. More specifically, our work and that of others have shown that neutrophils can contribute to M2 cell activation (Bosurgi et al., 2017; Chen et al., 2014). Therefore, we sought to assess whether the high Arg1 expression was also dependent on Nb-activated neutrophils. A role for neutrophils in the preferential activation of Mo-AMs would be consistent with a role for extrinsic signals in addition to intrinsic cell lineage differences contributing to differential macrophage subset activation in the lung. To test this possibility, *Cx3cr1*$^{\text{CreERT2-IRES-YFP/+}}$*Rosa26*$^{\text{floxed-tdTomato/+}}$ mice were administered TAM as described above, and an anti-Ly6G neutrophil-depleting antibody (Ab) or isotype control was administered at days −1, +1, and 3 after Nb inoculation. At day 7 after inoculation, total lung-cell suspensions were stained for AMs and analyzed by flow cytometry for tdTomato expression. Elevations in intracellular Arg1 protein expression (Figures 6D–6F) and gene expression (Figure 6G), as measured by RT-PCR, were significantly reduced in tdTomato^{+} Mo-AMs after neutrophil depletion.

Previous studies have shown that macrophage-mediated helminth killing is dependent on Arg enzymatic activity through the use of specific inhibitors (Chen et al., 2014; Obata-Ninomiya et al., 2013). We next examined macrophages from Arg1 conditional knockout mice, where macrophages were isolated from Tie2-Cre $Arg1^{fl/fl}$ or control Tie2-Cre mice at day 7 after inoculation and cultured with Nb L3. The use of Tie-2 to drive macrophage deletion of *Arg1* has significant advantages over LysM-Cre, which is ineffective at deleting *Arg1* in macrophages (Murray, 2017). As shown in Figures 7A and 7B, macrophages from Nb-primed Tie2-Cre $Arg1^{fl/fl}$ mice showed markedly impaired L3 killing and a corresponding increase in metabolic activity, as assessed by ATP worm levels. This is consistent with previous studies showing reduced impairment of *Heligmosomoides polygyrus* larval mobility by macrophages from Tie2-Cre$Arg1^{fl/fl}$ mice (Esser-von Bieren et al., 2013). However, it remained unknown how Arg1 actually affects parasitic nematode larval survival. Arg1 triggers a cascade of effects resulting in the production of potentially toxic urea and also polyamines, which can promote cellular activation and proliferation (Kreider et al., 2007). Recent studies of the intestinal and hepatic type 2 responses in schistosome-infected mice have further shown an important role for Arg1 in depleting local arginine concentrations and thereby attenuating activation of nearby immune cells, effectively resulting in immunosuppression (Pesce et al., 2009). Arginine depletion and not metabolite generation mediated the downregulatory effect (Van de Velde et al., 2017). Based on these findings, we hypothesized that one mechanism through which Arg1 may kill L3 would be through localized depletion of arginine, an essential amino acid for nematodes, as they are generally not thought to be capable of arginine biosynthesis (Tyagi et al., 2015; Zecic et al., 2019). To test whether L-arginine was depleted in the macrophage/L3 co-cultures, L-arginine was directly measured following a culture of L3 alone or a co-culture of exsheathed L3 with either naive lung macrophages or lung macrophages from mice inoculated with Nb for 7 days. Significant decreases in L-arginine were detected only in L3 co-cultures with lung macrophages from Nb-inoculated mice (Figure 7C). We next performed L-arginine add-back experiments to examine whether macrophage killing could be blocked by supplementing the media with highly purified L-arginine. As shown in Figures 7D and 7E, larval killing was significantly decreased, with increased L-arginine supplementation, and live parasite metabolic activity, as measured by ATP values, was markedly increased. To assess whether L-arginine was required for L3 survival under *in vitro* conditions, exsheathed larvae were cultured in arginine-free media. As shown in Figure 7F, parasite mortality was high in arginine-free media, while the addition of arginine significantly reduced mortality. Furthermore, supplementation of arginine-free media with exogenous L-arginine enhanced parasite ATP levels (Figure 7G). To examine whether anti-helminth functions of lung macrophages were specific to Nb, primed lung macrophages isolated at day 7 after Nb inoculation were co-cultured with a different nematode parasite, *H. polygyrus*. L3 mortality (Figure 7H) was markedly increased and was reduced by supplementation with L-arginine. Similarly reduced L3 ATP levels were markedly enhanced by L-arginine administration (Figure 7I). These studies thus indicate that Nb-primed macrophages are capable of killing other nematode parasite species and provide substantial insight into the protective mechanisms of M2 macrophages.

DISCUSSION

Macrophages mediate resistance to helminths as well as microbial pathogens. Recent studies suggest that the lung is an important target for therapeutic strategies and vaccine development against helminths (Harvie et al., 2010) and that lung macrophages with anti-helminth effector functions develop shortly after Nb infection (Chen et al., 2014). By tracking monocyte recruitment to the lungs and their differentiation in this microenvironment, we showed that during infection they can develop an AM-like phenotype that is distinct from TD-AMs, preferentially mediates helminth killing, and includes expression of high levels of Arg1, which is critical for helminth resistance. Development of this polarized Mo-AM phenotype was dependent on neutrophil help, and our studies further show that macrophage-derived Arg1 mediates parasite killing through the localized depletion of arginine, providing a nutrient deprivation mechanism for macrophage-mediated helminth killing.

Emerging studies have now demonstrated that macrophages exhibit tissue-specific phenotypes that are well-suited for their specific microenvironments (Aegerter et al., 2020; Glass and Natoli, 2016; Gundra et al., 2017; Okabe and Medzhitov, 2016). In the lung, TD-AMs play a critical role in lung homeostasis including clearance of debris and surfactant recycling (Hussell and Bell, 2014; Kopf et al., 2015). After Nb infection, the lung NAVMs are a heterogeneous population, with macrophages derived from monocytes and also TD interstitial macrophage populations (Ural et al., 2020). Our findings with the CCR2-DTR and CD45 transgenic mice indicate that the rapid increase in AMs observed after Nb infection is derived in part from monocyte-derived cells. Furthermore, these Mo-AMs are differentially activated with distinct effector functions including enhanced parasite killing and Arg1 expression, thereby explaining why NAVMs were less effective at killing the helminths *in vitro* but after transfer, in the context of the lung microenvironment, could develop this anti-helminth effector function associated with their expression of AM surface markers. Recent studies in a chimeric model showed that recruited Mo-AMs during influenza infection preferentially conferred protection against heterologous bacterial infections (Aegerter et al., 2020). Interestingly, fibrosis was also linked to a recruited Mo-AM population with increased Arg1 expression in an acute lung injury model (Misharin et al., 2017). Our studies now show that tracking of monocytes using fate-mapping mice under physiological conditions reveals their differentiation into Mo-AMs that are characterized by differentially high Arg1 expression and enhanced anti-helminth effector function.

Nb larva typically leave the lung and migrate to the small intestine by day 4 after inoculation (Anthony et al., 2007). The magnitude of the type 2 inflammatory response decreases shortly thereafter but remains potent, resulting in chronic inflammation and the associated development of fibrosis and emphysematous pathology (Chen et al., 2018; Marsland et al., 2008). Mo-AMs expressed high levels of CD11c and SiglecF by day 7, but transcriptome analyses revealed that they were distinct from TD-AMs. The observation that this population expressed considerably higher levels of Arg1 and other type 2-associated markers compared with TD-AMs indicates a distinct activation state and effector function. By day 14, gene expression of type 2 immune response genes was decreased in the TD-AMs but remained elevated in Mo-AMs. These findings are consistent with a model where TD-AMs revert

back to a housekeeping phenotype shortly after infection, likely to assume their critical function of maintaining homeostasis and healthy lung function (Hussell and Bell, 2014). In this context, as described in the results, PPARγ expression remained higher in TD-AMs at both days 7 and 14 after Nb inoculation relative to Mo-AMs. PPARγ mediates lipid metabolism, a critical homeostatic function of TD-AMs (Caputa et al., 2019; Hussell and Bell, 2014). However, our findings may also be consistent with recent findings that TD-AMs may undergo paralysis associated with poor phagocytic activity after bacterial infections (Roquilly et al., 2020). In contrast, AMs derived from monocytes maintain a more activated phenotype with a high expression of M2 markers and an associated remodeling of the chromatin landscape. As such, the Mo-AMs are likely primed to respond to subsequent helminth infections. In future studies, it will be interesting to examine the duration of changes in the chromatin landscape relative to gene expression, as these epigenetic modifications may potentially contribute to trained immunity, consistent with previous studies showing the persistence of trained macrophages as late as 45 days after Nb inoculation (Chen et al., 2014). These epigenetic changes in macrophages may also affect heterologous infections, consistent with previous studies that indicate Nb infection can enhance susceptibility to infection with *Mycobacterium tuberculosis* in part through impaired macrophage effector function (Potian et al., 2011). Interestingly, we also observed increases in macrophage expression of IL-13, which was confirmed by cytoplasmic IL-13 staining. Previous studies have also shown increased lung macrophage IL-13 production during type 2 responses, in some cases directly contributing to the polarization of the response (Wu et al., 2015; Yamaguchi et al., 2015). It is increasingly apparent that a number of different innate myeloid and lymphoid immune cells can express type 2 cytokines during allergic and anti-helminth responses, likely triggered by the activation of common pathways including IL-4R signaling (Gause et al., 2020), and potentially play essential or overlapping roles at different stages of the response.

After the primary infection, our findings show that several days elapse as the monocytes are recruited to the lung and differentiate to the AM phenotype. The Mo-AM population likely has little effect on parasite migration during a primary infection, consistent with most parasites successfully reaching the small intestine by day 4 after the primary inoculation. However, after infection, the Mo-AMs persist in the lung for prolonged periods, readily detected as late as 30 days after inoculation. As such, during a subsequent infection, parasites can encounter these primed macrophages in the lung, slowing their migration and eventually culminating in their morbidity and death in the lung over a period of several days, thereby blocking their migration to the intestine. Our findings further suggest that the Mo-AMs play a critical role in contributing to this accelerated resistance, likely through their heightened Arg1 activity, which depletes L-arginine levels. Consistent with this possibility, our confocal imaging studies further indicate that these Mo-AMs are in close proximity to Nb larvae, essentially surrounding these parasites in the lung after a second infection. The overall primed state of Mo-AMs may also play a significant role in infections with heterologous pathogens, potentially providing protective immunity or alternatively increased susceptibility, as has been observed with *Mycobacterium tuberculosis* infections (Potian et al., 2011). As such, heterogeneity between individuals in innate responses to specific pathogens may be potentially influenced by previous heterologous pathogen exposure.

Neutrophils are increasingly recognized as significant players in helminth infections and in cross talk with macrophages. Recent studies indicate that neutrophils exhibit a distinct alternatively activated (N2) phenotype during helminth infections (Chen et al., 2014) and that they can contribute resistance mechanisms leading to a reduced worm burden after the primary inoculation (Bouchery et al., 2020; Sutherland et al., 2014). Interactions of macrophages with neutrophils can promote M2 activation, likely through both production of type 2 cytokines and direct cell-cell interactions involving efferocytosis (Bosurgi et al., 2017; Chen et al., 2014). Also, in the lung environment, surfactant protein A can also promote M2 macrophage activation (Minutti et al., 2017). Interestingly antibodies are not required for resistance to Nb (Liu et al., 2010), although they do play an important role in resistance and in macrophage Arg1 expression during *H. polygyrus* infection (Esser-von Bieren et al., 2013; Liu et al., 2010). The lung tissue microenvironment, including neutrophil interactions, thus provides sufficient signals for M2 macrophage activation even in the absence of Ab signaling. Effects of neutrophil-macrophage cross talk in driving activation and the associated effector functions of these myeloid cells can play a significant role in immune responses against diverse pathogens (Espinosa et al., 2017). Our findings indicate that neutrophils are critical for the polarization of the Mo-AM subset toward elevated expression of type 2 markers, including Arg1. Our finding that neutrophils preferentially stimulate this phenotype in recruited Mo-AMs indicates that both intrinsic lineage-specific activation signatures and extrinsic signals provided in the inflamed lung tissue microenvironment interact to drive their activation, culminating in an anti-helminth effector phenotype.

Although previous studies have identified Arg as being essential in macrophage-mediated helminth killing in the skin (Obata-Ninomiya et al., 2013), lung (Chen et al., 2014), and small intestine (Anthony et al., 2006; Esser-von Bieren et al., 2013), the mechanism through which this enzyme mediates this effect has remained unknown. Our studies now reveal a mechanism that is independent of the many molecules produced during the Arg1 cascade, culminating in the production of urea, ornithine, and polyamines. Our findings do not exclude other mechanisms involving the Arg1 pathways or potentially other molecules produced independently of Arg1. However, our studies do indicate that Arg1-mediated l-arginine depletion is essential in macrophage-mediated killing of L3. The production of high levels of Arg1 by the Mo-AM subset as they surround the invading parasitic larvae likely deprives the parasite of arginine. We now specifically show that Nb metabolism is slowed and that mortality markedly increased in the absence of an external source of arginine in Nb larval cultures with primed M2 macrophages. The developing L3 likely obtains this essential amino acid from the vertebrate host as it traffics through various tissues *in vivo*. The ability of the activated M2 macrophage to adhere to the invading L3 results in a localized depletion of this critical nutrient, effectively providing a potent anti-helminth effector mechanism. Our finding that arginine supplementation was sufficient to block macrophage-mediated killing indicates the potent effect of this anti-helminth macrophage effector mechanism. Given the intense selection pressure of helminths on vertebrate evolution, one can postulate that the high level of Arg1 produced by M2 macrophages, specifically helminth-activated Mo-AMs, may in part be an adaptation resulting in a potent resistance mechanism against these multicellular pathogens. In contrast, Arg1 does not appear to significantly impact lung

immune cell activation and inflammation during type 2 responses, including schistosome-egg-induced granuloma formation (Barron et al., 2013). It is intriguing that in microbial infections, arginine also plays a critical role in resistance through generation of nitric oxide synthase 2 activity resulting in the production of anti-microbial nitric oxide. As such, arginine metabolism thus plays an important role in mediating resistance against eukaryotic as well as microbial pathogens, although the mechanisms contributing to the protective response are distinct. The mechanism of Arg1-mediated resistance is indeed more similar to Arg1-mediated suppression of Th2 cell activation, where nutrient depletion also plays a major role (Pesce et al., 2009).

However, it is likely that *in vivo* there are multiple mechanisms contributing to host resistance against helminth infection, which may vary with different tissue microenvironments. Taken together, our studies now indicate a significant role for nutrient depletion by a specific Mo-mac subset, and it will be important in future studies to examine how this resistance mechanism interacts with other components of the armamentarium contributing to host protection.

Limitations of the study

A limitation of these studies is that they do not distinguish whether the macrophages passively adhere to the parasite as it migrates through the lung, with the larvae then trapped in aggregates of macrophages that formed following previous infections, or whether the macrophages actively swarm the parasite. It should be also noted that increased Mo-AM activation including expression of additional genes associated with type 2 immunity, besides Arg1, may also trigger other effector mechanisms contributing to anti-helminth effects. Future experiments involving imaging in living tissue and the characterization of additional anti-helminth effector mechanisms are thus needed.

The genetic background of the host may also be of importance, and our studies of Mo-AMs have necessarily focused on BL/6 mice, as that is the genetic background of the fate-mapping mice used in these studies. Previous studies have shown potent type 2 responses to Nb occur in both BL/6 and BALB/c mice (Bouchery et al., 2015, 2020; Chen et al., 2012, 2014, 2018). However, a limitation of the studies described in this paper is that they have been performed only in the BL/6 strain of mouse under conventional animal housing conditions. In future studies, the role of Mo-AMs in mediating helminth resistance in mice with varying genetic backgrounds, or those housed in different environments (Yeung et al., 2020), should be investigated.

STAR★METHODS

RESOURCE AVAILABILITY

Lead contact—Further information and requests for resources and reagents should be directed to and will be fulfilled by the lead contact, William C. Gause (gausewc@njms.rutgers.edu).

Materials availability—This study did not generate unique reagents.

Data and code availability—The datasets generated, RNA-seq, and ATAC-seq, have been deposited in GEO and dbGAP and are publicly available. Accession numbers are listed in the key resources table. This paper does not report original code. Any additional information required to access and analyze the data reported in this paper is available from the lead contact upon request.

EXPERIMENTAL MODEL AND SUBJECT DETAILS

Mice—BALB/c ByJ (CD45.1), BALB/c (CD45.2), BL/6 mice were purchased from The Jackson Laboratory (Bar Harbor, ME) and CCR2-DTR, CCR2-GFP, Tie 2-Cre and Tie2-Cre $Arg^{fl/fl}$ mice were all bred and maintained in a specific pathogen-free, virus Ab-free facility at Rutgers New Jersey Medical School Comparative Medicine Resources. Healthy 8–12 week old male and female mice were selected for treatment groups from purchased or bred colonies, without using specific randomization methods or specific blinding methods. The studies have been reviewed and approved by the Institutional Animal Care and Use Committee at Rutgers-the State University of New Jersey. The experiments herein were conducted according to the principles set forth in the Guide for the Care and Use of Laboratory Animals, Institute of Animal Resources, National Research Council, Department of Health, Education and Welfare (US National Institutes of Health).

METHOD DETAILS

Parasite culture, inoculation of mice, and neutrophil depletion—*N. brasiliensis* (Nb) L3 were maintained in a petri dish culture containing charcoal and sphagnum moss. The larvae were isolated from cultures using a modified Baermann apparatus with 400U penicillin, 400 μg ml^{-1} streptomycin, and 400 μg ml^{-1} Neomycin (GIBCO, Rockville, MD) in sterile PBS, and then washed with sterile PBS three times. Mice were inoculated subcutaneously with a 40 μl suspension of 650 Nb L3. For *H. polygyrus*, after propagation, L3 larvae were maintained in PBS at 4°C. For neutrophil depletion, Ly6G-specific antibody (BioXcell, West Lebanon, NH) or isotype control IgG (BioXcell) was administered to mice both intraperitoneally (0.3 mg in 0.2 ml) and intratracheally (0.2 mg in 0.05 ml) 1 day before and 3 or 7 days after parasite inoculation, as described previously (Chen et al., 2014).

Flow cytometry and adoptive transfer—Lung tissue was washed with stirring at room temperature for 10 min in Hank's balanced salt solution (HBSS) with 1.3 mM EDTA (Invitrogen), then minced and treated at 37°C for 30 min. with collagenase (1 mg / ml; Sigma) in RPMI1640 with 10% fetal calf serum (FCS) and with 100 μg / ml of DNase for 10 min. Cells were lysed with ACK (Lonza, Walkersville, MD) to remove erythrocytes. Cells were blocked with Fc Block (BD Biosciences, San Jose, CA), directly stained with fluorochrome-conjugated antibodies against CD45,F4/80, CD64, CD11c, Siglec-F,CD11b,Ly6C, and analyzed by flow cytometry. For adoptive transfer, macrophages ($F4/80^{+}CD64^{+}SiglecF^{vari}CD11c^{vari}$), alveolar macrophages (AMs) ($F4/80^{+}CD64^{+}SiglecF^{+}CD11c^{hi}$), or nonalveolar macrophages (NAVMs) ($F4/80^{+}CD64^{+}SiglecF^{-}CD11c^{vari}$), were electronically sort purified (>98%), 5 million cells were transferred i.t. into recipient mice. Two days after cell transfer, the recipients were inoculated with Nb L3. For *Cx3cr1*$^{CreERT2\text{-}IRES\text{-}YFP}$ x *Rosa26*$^{floxed\text{-}tdTomato}$ reporter mice, tamoxifen (75 mg/kg body weight, Sigma, cat#T5648) were delivered to mice

at days −1, and +1 after Nb inoculation. At different timepoints after inoculation, single cells were isolated from whole lung and directly stained with fluorochrome-conjugated antibodies against CD45, F4/80, CD64, CD11c, Siglec-F and analyzed by flow cytometry. Cells were gated on $CD45^+$,$F4/80^+$,$CD64^+$ cells, then further gated on Siglec-F^+, $CD11c^{hi}$ AMs. AMs were separated into $tdTomato^+$ monocyte-derived alveolar macrophages (Mo-AMs) and $tdTomato^-$ alveolar macrophages (TD-AMs). For intracellular staining of Arg1, cells were first surface stained and then fixed and permeabilized using a kit from BD BioSciences (cat# 554714). For cytospin analyses, sorted cells (2×10^5) from lung tissue were suspended in 200 μl of 1x PBS with 2.5% FCS. The sorted cell suspensions were loaded into a Shandon Cytospin 4 (Thermo Electron Corporation, Waltham, MA), spun at 800–1000 rpm for 5 min and stored at −80°C. Frozen cytospin slides were thawed at room temperature for 30 min, fixed in 4% PFA for 15 min, and stained with an APC-conjugated antibody specific to Arginase 1 or corresponding isotype control (Bioss Inc., Woburn, MA). Coverslips were applied to the slides using Vectashield mounting medium (Vector Laboratories, Burlingame, CA) with DAPI. Images were taken using a Leica DM6000B fluorescent microscope, Orca Flash 4.0 mounted digital camera (Hamamatsu Photonics K.K., Japan) and LAS Advanced Fluorescence software (Leica Microsystems, Buffalo Grove, IL). Fluorescent channels were photographed separately and then merged. Exposure times and fluorescence intensities were normalized to appropriate control images.

Confocal microscopy—$Cx3cr1^{CreERT2\text{-}IRES\text{-}YFP/+}Rosa26^{floxed\text{-}tdTomato/+}$ received tamoxifen at day −1 and +1 after primary Nb inoculation of 500 L3. At day 2 after primary inoculation, mice were given a second inoculation of 250. Lung tissues were then collected at day 6 after primary inoculation. This regimen was found to optimize visualization of migrating parasites interacting with primed macrophages. Lung tissues were fixed in 1% paraformaldehyde overnight at 4°C. Tissues were washed with 5 mM NH_4Cl and incubated in 30% (w/v) sucrose overnight at 4°C. Lung tissue was embedded in Optimal Cutting Temperature Compound (Tissue-Tek) and 5 μm sections were cut on CM1950 Cyrostat (Leica, Weltzlar, Germany). Sections were blocked with 1% Rat serum and 1% FcBlock in PBS for 1 hr, followed by 5ug/ml of anti-CD11c-APC overnight and sealed with ProLong Gold Antifade (Invitrogen, Waltham, MA). Confocal Images were captured using a Nikon A1R SI confocal microscope with the DUG GaAsP detector. 10x Plan Apo Lambda N.A. 0.45, 20x Plan Apo VC N.A. 0.75 and 60x Plan Apo VC N.A. 1.4 objectives were used along with DIC optics for the transmitted light images.

Electron microscopy—Samples were fixed in 2.5% glutaraldehyde / 4% paraformaldehyde in 0.1M cacodylate buffer and then post-fixed in buffered 1% osmium tetroxide. Samples were subsequently dehydrated in a graded series of acetone and embedded in Embed812 resin. 90 nm thin sections were cut on a Leica UC6 ultramicrotome and stained with saturated solution of uranyl acetate and lead citrate. Images were captured with an AMT (Advanced Microscopy Techniques) XR111 digital camera at 80Kv on a Philips CM12 transmission electron microscope.

Macrophage co-cultures with parasitic L3—Macrophages, alveolar macrophages, or nonalveolar macrophages, were electronically sorted from mice inoculated with Nb for 7

days, and placed on 12-well plates (1×10^6) in 2 ml of RPMI1640 medium with 10% of FBS, 400U penicillin, 400 μg/ml streptomycin, and 100 μg/ml gentamycin. 100 μl of serum from the donor mice was also added to medium. One hundred exsheathed L3 larvae were added to each well. Cells and worms were co-cultured for 5 days at 37°C. The procedure to ex-sheath larvae included incubation of L3 with 6.7 mM sodium hypochlorite in PBS for 15 min. at room temperature, washing the L3 six times with sterile PBS containing 400U penicillin and 400 μg ml−1 streptomycin. To ex-sheath Hp L3, the larvae were maintained in phenol RPMI1640 with 10% FBS at 37°C, and CO_2 was added to the medium until yellow color obtained, and then incubated for 25hrs in CO_2 incubator. The ex-sheathed larvae were isolated using a modified Baermann apparatus with 400U penicillin, 400 μg ml^{-1} streptomycin, and 400 μg ml^{-1} Neomycin (GIBCO, Rockville, MD) in sterile PBS, and then washed with sterile PBS three times. In some experiments, the L3 were cultured in L-arginine free RPMI1640 (Thermofisher) without cells and in some groups commercial L-arginine was added to the medium. To remove adherent macrophages from L3 after co-culture, 20 L3 were picked from cultures using a p1000 pipetman, washed in PBS, and then incubated in PBS with 0.5 mM EDTA for 1hr, as described previously(Chen et al., 2014).

The ATP levels for the L3 were performed according to the manufacturer's instructions. Briefly, 20 Nb L3 were collected with 100 μl of PBS and 100 μl of the Celltiter-Glo Luminescent reagent (Promega, Madison, WI) was then added. The larvae were homogenized and incubated for five minutes at room temperature to stabilize the luminescence signal. After the homogenate was centrifuged at 1000 g for 2 minutes, 100 μl of supernatant was applied to the luminometer to measure luminescence. As a negative control, larvae in RPMI1640 medium were treated in boiling water for five minutes and after cooling, the worms were homogenized with reagent. Dead larvae after incubation with macrophages were defined as non-motile, outstretched bodies, with non-refractive internal structures. L-arginine was measured using an L-arginine assay kit (Abcam, cat#ab252892),

Cytokine gene expression by RT-PCR—For qPCR, RNA was extracted from lung tissue or sorted macrophages and reverse transcribed to cDNA. qPCR was done with Taqman (Life Technologies Corporation, Carlsbad, CA) kits and the Applied Biosystems QuantStudio 6 Flex Real-Time PCR System. All data were normalized to 18S ribosomal RNA, and the quantification of differences between treatment groups was calculated according to the manufacturer's instructions. Gene expression is presented as the fold increase over naïve WT controls.

RNA sequencing—Alveolar macrophages from *Cx3*cr1$^{CreERT2\text{-}IRES\text{-}YFP/+}$Rosa26$^{floxed\text{-}tdTomato/+}$ Nb- inoculated mice were sort-purified by gating on $CD45^+$,$CD64^+$,F4/80+,$CD11c^+$,$Siglec\text{-}F^+$ AMs then sorted based on tdTomato expression, with TD-AMs being tdT^- and Mo-AMs tdT^+. Cells from a minimum of three biological replicates were sorted and pooled. The purity of all cell populations was 98% or greater. RNA was extracted using the RNeasy Plus Micro Kit (catalog no. 74034; QIAGEN). Illumina-compatible libraries were generated using the NEBNext Ultra II DNA Library Prep Kit for Illumina (catalog no. E7645S; New England BioLabs) and

sequenced using an Illumina NovaSeq 6000 system in a paired-end 2×50-base pair (bp) reads configuration. Bulk RNA-seq analysis was performed in accordance with the nf-core RNA-seq guidelines v.1.4.2 (Ewels et al., 2020). Briefly, the output reads were aligned to the GRCm38 (mm10) genome using STAR, followed by gene count generation using feature Counts and StringTie (Dobin et al., 2013; Liao et al., 2014; Pertea et al., 2015). Read counts were normalized and compared between groups for differential gene expression using DESeq2 with significance cutoff at false discovery rate-adjusted $p<0.05$ (Love et al., 2014). Determination of functional pathways was performed using Ingenuity Pathway Analysis (IPA) on differentially expressed genes.

Assay for transposase-accessible chromatin with sequencing (ATAC-seq)— Sorted cells were lysed in buffer (10 mM Tris-HCl, 10 mM NaCl, 3 mM $MgCl_2$, 0.1% octylphenoxypolyethoxyethanol, 0.1% digitonin and 0.1%IPGAL) for 3 min at 4°C and then washed with lysis buffer without digitonin or IPGAL and centrifuged and resuspended with transposase reaction mix (Ilumina Nextera), and incubated for 30 min at 37°C. Cells were then PCR amplified in KAPA HiFi 2× mix (Kapa Biosystems) with barcoding primers. Amplification was conducted for 45 s at 98°C, followed by five cycles of denaturing at 98°C for 15 s, annealing at 63°C for 30 s, extension at 72°C for 30 s, and a final extension of 72°C for 1 min in a thermal cycler (MX4005P). Quantitative PCR library amplification test and PCR library amplification were performed as previously described (Weinstein et al., 2018). Sequencing reads were trimmed (TrimGalore v0.6.4) and aligned to the reference genome (GRCm38) using BWA (v0.7.17). Subsequent QC and filtering was performed using picard (v2.23.1), SAMtools (v1.10), BEDtools (v2.29.2), and BAMtools (v2.5.1), followed by peak calling using MACS2 (v2.2.7.1) and annotation via HOMER (v4.11). Statistically significant differential peaks were identified between groups using DESeq2 (v1.26) and visualized using R.

Seahorse assay for metabolic activity— *Cx3*cr1$^{\text{CreERT2-IRES-YFP/+}}$Rosa26$^{\text{floxed-tdTomato/+}}$ and CX3CR1-cre mice (control group) received tamoxifen at one day before and one day after Nb inoculation (−1, +1 day) and were sacrificed at day 7. Lung single cells were isolated and td tomato+ and td tomato- alveolar macrophages from reporters or alveolar macrophages from control group mice were sorted via flow cytometry. Alveolar macrophages (~75,000 cells/well) from each group were seeded into CellTak (Corning, # 354240) coated XFp plates in XF RPMI complete assay media, and incubated at 37° C without CO_2 for 45 minutes. The assay was run on a Seahorse XFp Extracellular Flux Analyzer with each group of AMs run in duplicate. After 20 cycles of basal measurement, Rotenone and Antimycin A (Seahorse XF Cell Mito Stress Kit), inhibitors of mitochondrial complex I and III, respectively, were injected into each well for a final concentration of 0.5 uM/well. Oxidative phosphorylation was measured by the oxygen consumption rate (OCAR; pmol/min) while glycolysis was measured by the extracellular acidification rate (ECAR; mpH/min) due to the accumulation of lactate or other metabolic acids and release of protons into the extracellular medium.

5-Ethynyl-2'-deoxyuridine (EdU) incorporation assay— *Cx3*cr1$^{\text{CreERT2-IRES-YFP/+}}$Rosa26$^{\text{floxed-tdTomato/+}}$ mice received tamoxifen at one day before

and one day after Nb inoculation (−1, +1 day), and received Edu (5 mg/ml, 100 ul, i.p.) every other day starting from one day before Nb inoculation ((−1, +1, +3, +5 day) and sacrificed at day 7. Control groups received tamoxifen and Edu but were not inoculated with Nb. Lung macrophages were stained with fluorochrome-conjugated antibodies against CD45, F4/80, CD64, CD11c, Siglec-F, then Edu incorporation was assessed using Click-iT Edu flow cytometry cell proliferation assay kit (ThermoFisher Scientific, cat#C10424).

QUANTIFICATION AND STATISTICAL ANALYSIS

Data were analyzed using the statistical software program Prism 8 (GraphPad Software, Inc., La Jolla, CA) and are reported as means (± SEM). Differences between two groups were assessed by student's T-test, differences among multiple groups were assessed by one way ANOVA and individual comparisons were analyzed using Holm-Sidak test. Differences of $p < 0.05$ were considered statistically significant.

Supplementary Material

Refer to Web version on PubMed Central for supplementary material.

ACKNOWLEDGMENTS

This research was supported by National Institutes of Health (NIH) grants R01DK113790 (W.C.G.), RO1 AI1344040 (W.C.G.), R01AI131634 (M.C.S. and W.C.G.), RO1 AI123224 (M.C.S.), and R01 AI143861 (K.K.). J.J.P. and D.W.E.-N. are supported by T32AI125185. J.J.P., K.L., and D.W.E.-N. are supported by T32AI125185.

REFERENCES

Aegerter H, Kulikauskaite J, Crotta S, Patel H, Kelly G, Hessel EM, Mack M, Beinke S, and Wack A (2020). Influenza-induced monocyte-derived alveolar macrophages confer prolonged antibacterial protection. Nat. Immunol 21, 145–157. [PubMed: 31932810]

Anthony RM, Urban JF Jr., Alem F, Hamed HA, Rozo CT, Boucher JL, Van Rooijen N, and Gause WC (2006). Memory T(H)2 cells induce alternatively activated macrophages to mediate protection against nematode parasites. Nat. Med 12, 955–960. [PubMed: 16892038]

Anthony RM, Rutitzky LI, Urban JF Jr., Stadecker MJ, and Gause WC (2007). Protective immune mechanisms in helminth infection. Nat. Rev. Immunol 7, 975–987. [PubMed: 18007680]

Barron L, Smith AM, El Kasmi KC, Qualls JE, Huang X, Cheever A, Borthwick LA, Wilson MS, Murray PJ, and Wynn TA (2013). Role of arginase 1 from myeloid cells in th2-dominated lung inflammation. PLoS one 8, e61961. [PubMed: 23637937]

Bleriot C, Chakarov S, and Ginhoux F (2020). Determinants of resident tissue macrophage identity and function. Immunity 52, 957–970. [PubMed: 32553181]

Bosurgi L, Cao YG, Cabeza-Cabrerizo M, Tucci A, Hughes LD, Kong Y, Weinstein JS, Licona-Limon P, Schmid ET, Pelorosso F, et al. (2017). Macrophage function in tissue repair and remodeling requires IL-4 or IL-13 with apoptotic cells. Science 356, 1072–1076. [PubMed: 28495875]

Bouchery T, Kyle R, Camberis M, Shepherd A, Filbey K, Smith A, Harvie M, Painter G, Johnston K, Ferguson P, et al. (2015). ILC2s and T cells cooperate to ensure maintenance of M2 macrophages for lung immunity against hookworms. Nat. Commun 6, 6970. [PubMed: 25912172]

Bouchery T, Moyat M, Sotillo J, Silverstein S, Volpe B, Coakley G, Tsourouktsoglou TD, Becker L, Shah K, Kulagin M, et al. (2020). Hookworms evade host immunity by secreting a deoxyribonuclease to degrade neutrophil extracellular traps. Cell Host Microbe 27, 277–289 e276. [PubMed: 32053791]

Caputa G, Castoldi A, and Pearce EJ (2019). Metabolic adaptations of tissue-resident immune cells. Nat. Immunol 20, 793–801. [PubMed: 31213715]

Chen F, Liu Z, Wu W, Rozo C, Bowdridge S, Millman A, Van Rooijen N, Urban JF Jr., Wynn TA, and Gause WC (2012). An essential role for TH2-type responses in limiting acute tissue damage during experimental helminth infection. Nat. Med 18, 260–266. [PubMed: 22245779]

Chen F, Wu W, Millman A, Craft JF, Chen E, Patel N, Boucher JL, Urban JF Jr., Kim CC, and Gause WC (2014). Neutrophils prime a long-lived effector macrophage phenotype that mediates accelerated helminth expulsion. Nat. Immunol 15, 938–946. [PubMed: 25173346]

Chen F, Wu W, Jin L, Millman A, Palma M, El-Naccache DW, Lothstein KE, Dong C, Edelblum KL, and Gause WC (2018). B cells produce the tissue-protective protein RELMalpha during helminth infection, which inhibits IL-17 expression and limits emphysema. Cell Rep 25, 2775–2783 e3. [PubMed: 30517865]

Dobin A, Davis CA, Schlesinger F, Drenkow J, Zaleski C, Jha S, Batut P, Chaisson M, and Gingeras TR (2013). STAR: ultrafast universal RNA-seq aligner. Bioinformatics 29, 15–21. [PubMed: 23104886]

Espinosa V, Dutta O, McElrath C, Du P, Chang YJ, Cicciarelli B, Pitler A, Whitehead I, Obar JJ, Durbin JE, et al. (2017). Type III interferon is a critical regulator of innate antifungal immunity. Sci. Immunol 2, eaan5357. [PubMed: 28986419]

Esser-von Bieren J, Mosconi I, Guiet R, Piersgilli A, Volpe B, Chen F, Gause WC, Seitz A, Verbeek JS, and Harris NL (2013). Antibodies trap tissue migrating helminth larvae and prevent tissue damage by driving IL-4Ralpha-independent alternative differentiation of macrophages. PLoS Pathog 9, e1003771. [PubMed: 24244174]

Ewels PA, Peltzer A, Fillinger S, Patel H, Alneberg J, Wilm A, Garcia MU, Di Tommaso P, and Nahnsen S (2020). The nf-core framework for community-curated bioinformatics pipelines. Nat. Biotechnol 38, 276–278. [PubMed: 32055031]

Gause WC, Wynn TA, and Allen JE (2013). Type 2 immunity and wound healing: evolutionary refinement of adaptive immunity by helminths. Nat. Rev. Immunol 13, 607–614. [PubMed: 23827958]

Gause WC, Rothlin C, and Loke P (2020). Heterogeneity in the initiation, development and function of type 2 immunity. Nat. Rev. Immunol 20, 603–614. [PubMed: 32367051]

Glass CK, and Natoli G (2016). Molecular control of activation and priming in macrophages. Nat. Immunol 17, 26–33. [PubMed: 26681459]

Gundra UM, Girgis NM, Ruckerl D, Jenkins S, Ward LN, Kurtz ZD, Wiens KE, Tang MS, Basu-Roy U, Mansukhani A, et al. (2014). Alternatively activated macrophages derived from monocytes and tissue macrophages are phenotypically and functionally distinct. Blood 123, e110–e122. [PubMed: 24695852]

Gundra UM, Girgis NM, Gonzalez MA, San Tang M, Van Der Zande HJP, Lin JD, Ouimet M, Ma LJ, Poles J, Vozhilla N, et al. (2017). Vitamin A mediates conversion of monocyte-derived macrophages into tissue-resident macrophages during alternative activation. Nat. Immunol 18, 642–653. [PubMed: 28436955]

Harvie M, Camberis M, Tang SC, Delahunt B, Paul W, and Le Gros G (2010). The lung is an important site for priming CD4 T-cell-mediated protective immunity against gastrointestinal helminth parasites. Infect. Immun 78, 3753–3762. [PubMed: 20605978]

Hussell T, and Bell TJ (2014). Alveolar macrophages: plasticity in a tissue-specific context. Nat. Rev. Immunol 14, 81–93. [PubMed: 24445666]

Jenkins SJ, Ruckerl D, Cook PC, Jones LH, Finkelman FD, van Rooijen N, MacDonald AS, and Allen JE (2011). Local macrophage proliferation, rather than recruitment from the blood, is a signature of TH2 inflammation. Science 332, 1284–1288. [PubMed: 21566158]

Katona IM, Urban JF Jr., and Finkelman FD (1988). The role of L3T4+ and Lyt-2+ T cells in the IgE response and immunity to Nippostrongylus brasiliensis. J. Immunol 140, 3206–3211. [PubMed: 2966208]

Kopf M, Schneider C, and Nobs SP (2015). The development and function of lung-resident macrophages and dendritic cells. Nat. Immunol 16, 36–44. [PubMed: 25521683]

Kreider T, Anthony RM, Urban JF Jr., and Gause WC (2007). Alternatively activated macrophages in helminth infections. Curr. Opin. Immunol 19, 448–453. [PubMed: 17702561]

Liao Y, Smyth GK, and Shi W (2014). featureCounts: an efficient general purpose program for assigning sequence reads to genomic features. Bioinformatics 30, 923–930. [PubMed: 24227677]

Liu Q, Kreider T, Bowdridge S, Liu Z, Song Y, Gaydo AG, Urban JF Jr., and Gause WC (2010). B cells have distinct roles in host protection against different nematode parasites. J. Immunol 184, 5213–5223. [PubMed: 20357259]

Love MI, Huber W, and Anders S (2014). Moderated estimation of fold change and dispersion for RNA-seq data with DESeq2. Genome Biol 15, 550. [PubMed: 25516281]

Marsland BJ, Kurrer M, Reissmann R, Harris NL, and Kopf M (2008). Nippostrongylus brasiliensis infection leads to the development of emphysema associated with the induction of alternatively activated macrophages. Eur. J. Immunol 38, 479–488. [PubMed: 18203142]

Minutti CM, Jackson-Jones LH, Garcia-Fojeda B, Knipper JA, Sutherland TE, Logan N, Ringqvist E, Guillamat-Prats R, Ferenbach DA, Artigas A, et al. (2017). Local amplifiers of IL-4Ralpha-mediated macrophage activation promote repair in lung and liver. Science 356, 1076–1080. [PubMed: 28495878]

Misharin AV, Morales-Nebreda L, Reyfman PA, Cuda CM, Walter JM, McQuattie-Pimentel AC, Chen CI, Anekalla KR, Joshi N, Williams KJN, et al. (2017). Monocyte-derived alveolar macrophages drive lung fibrosis and persist in the lung over the life span. J. Exp. Med 214, 2387–2404. [PubMed: 28694385]

Murray PJ (2017). Macrophage polarization. Annu. Rev. Physiol 79, 541–566. [PubMed: 27813830]

Obata-Ninomiya K, Ishiwata K, Tsutsui H, Nei Y, Yoshikawa S, Kawano Y, Minegishi Y, Ohta N, Watanabe N, Kanuka H, et al. (2013). The skin is an important bulwark of acquired immunity against intestinal helminths. J. Exp. Med 210, 2583–2595. [PubMed: 24166714]

Okabe Y, and Medzhitov R (2016). Tissue biology perspective on macrophages. Nat. Immunol 17, 9–17. [PubMed: 26681457]

Parkhurst CN, Yang G, Ninan I, Savas JN, Yates JR 3rd, Lafaille JJ, Hempstead BL, Littman DR, and Gan WB (2013). Microglia promote learning-dependent synapse formation through brain-derived neurotrophic factor. Cell 155, 1596–1609. [PubMed: 24360280]

Pertea M, Pertea GM, Antonescu CM, Chang TC, Mendell JT, and Salzberg SL (2015). StringTie enables improved reconstruction of a transcriptome from RNA-seq reads. Nat. Biotechnol 33, 290–295. [PubMed: 25690850]

Pesce JT, Ramalingam TR, Mentink-Kane MM, Wilson MS, El Kasmi KC, Smith AM, Thompson RW, Cheever AW, Murray PJ, and Wynn TA (2009). Arginase-1-expressing macrophages suppress Th2 cytokine-driven inflammation and fibrosis. PLoS Pathog 5, e1000371. [PubMed: 19360123]

Potian JA, Rafi W, Bhatt K, McBride A, Gause WC, and Salgame P (2011). Preexisting helminth infection induces inhibition of innate pulmonary anti-tuberculosis defense by engaging the IL-4 receptor pathway. J. Exp. Med 208, 1863–1874. [PubMed: 21825018]

Roquilly A, Jacqueline C, Davieau M, Molle A, Sadek A, Fourgeux C, Rooze P, Broquet A, Misme-Aucouturier B, Chaumette T, et al. (2020). Alveolar macrophages are epigenetically altered after inflammation, leading to long-term lung immunoparalysis. Nat. Immunol 21, 636–648. [PubMed: 32424365]

Scott CL, Henri S, and Guilliams M (2014). Mononuclear phagocytes of the intestine, the skin, and the lung. Immunol. Rev 262, 9–24. [PubMed: 25319324]

Sutherland TE, Logan N, Ruckerl D, Humbles AA, Allan SM, Papayannopoulos V, Stockinger B, Maizels RM, and Allen JE (2014). Chitinase-like proteins promote IL-17-mediated neutrophilia in a tradeoff between nematode killing and host damage. Nat. Immunol 15, 1116–1125. [PubMed: 25326751]

Tyagi R, Rosa BA, Lewis WG, and Mitreva M (2015). Pan-phylum comparison of nematode metabolic potential. PLoS Negl. Trop. Dis 9, e0003788. [PubMed: 26000881]

Ural BB, Yeung ST, Damani-Yokota P, Devlin JC, de Vries M, Vera-Licona P, Samji T, Sawai CM, Jang G, Perez OA, et al. (2020). Identification of a nerve-associated, lung-resident interstitial macrophage subset with distinct localization and immunoregulatory properties. Sci. Immunol 5, eaax8756. [PubMed: 32220976]

Van de Velde LA, Subramanian C, Smith AM, Barron L, Qualls JE, Neale G, Alfonso-Pecchio A, Jackowski S, Rock CO, Wynn TA, et al. (2017). T cells encountering myeloid cells programmed

for amino acid-dependent immunosuppression use Rictor/mTORC2 protein for proliferative check-point decisions. J. Biol. Chem 292, 15–30. [PubMed: 27903651]

Weinstein JS, Laidlaw BJ, Lu Y, Wang JK, Schulz VP, Li N, Herman EI, Kaech SM, Gallagher PG, and Craft J (2018). Correction: STAT4 and T-bet control follicular helper T cell development in viral infections. J. Exp. Med 215, 999. [PubMed: 29440270]

Wu K, Byers DE, Jin X, Agapov E, Alexander-Brett J, Patel AC, Cella M, Gilfilan S, Colonna M, Kober DL, et al. (2015). TREM-2 promotes macrophage survival and lung disease after respiratory viral infection. J. Exp. Med 212, 681–697. [PubMed: 25897174]

Yamaguchi R, Yamamoto T, Sakamoto A, Ishimaru Y, Narahara S, Sugiuchi H, Hirose E, and Yamaguchi Y (2015). Mechanism of interleukin-13 production by granulocyte-macrophage colony-stimulating factor-dependent macrophages via protease-activated receptor-2. Blood Cells Mol. Dis 55, 21–26. [PubMed: 25976462]

Yeung F, Chen YH, Lin JD, Leung JM, McCauley C, Devlin JC, Hansen C, Cronkite A, Stephens Z, Drake-Dunn C, et al. (2020). Altered immunity of laboratory mice in the natural environment is associated with fungal colonization. Cell Host Microbe 27, 809–822 e806. [PubMed: 32209432]

Zecic A, Dhondt I, and Braeckman BP (2019). The nutritional requirements of Caenorhabditis elegans. Genes Nutr 14, 15. [PubMed: 31080524]

Highlights

- Helminth infection promotes a restructuring of myeloid cells in the lung
- Highly activated monocyte-derived macrophages populate the lung post-infection
- These macrophages express alveolar macrophage markers and elevated levels of Arg1
- Arg1 mediates helminth killing through localized depletion of arginine

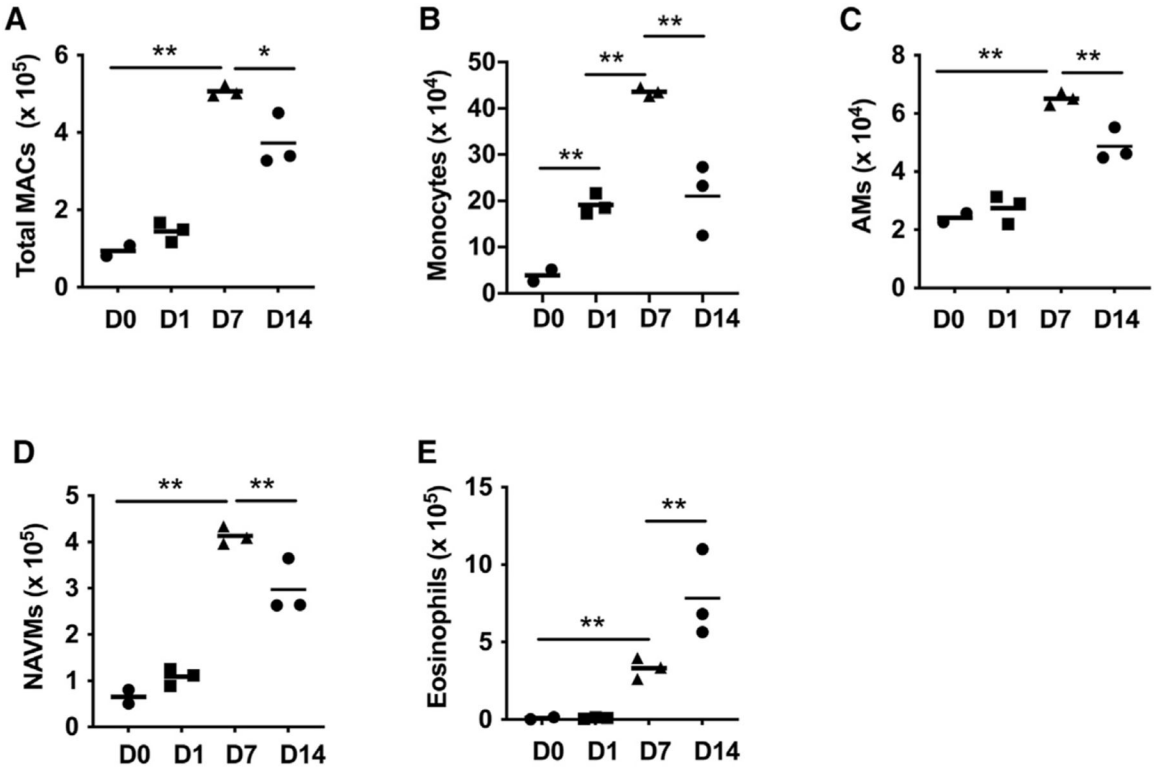

Figure 1. Substantial changes in lung macrophage subsets occur after *N. brasiliensis* inoculation

(A–E) Flow cytometric analysis of macrophage subsets obtained from single-cell suspensions of two lung lobes from BALB/c mice at days 1, 7, and 14 after *N. brasiliensis* inoculation. Total numbers of lung macrophages ($CD64^+$, $F4/80^+$, $CD11c^{var}$) (A); monocytes ($CD11b^+$, $Ly6C^+$) (B); alveolar macrophages (AMs) (CD64+, F4/80+, SiglecF+, CD11c+) (C); non-AMs (NAVMs) ($CD64^+$, $F4/80^+$, $SiglecF^-$, $CD11c^{var}$) (D); and eosinophils ($F4/80^+$, $SiglecF^+$, $CD11c^-$) (E).

Each symbol represents an individual mouse and horizontal lines indicate the mean. All results are representative of two independent experiments. *$p < 0.05$, **$p < 0.01$ (one-way ANOVA).

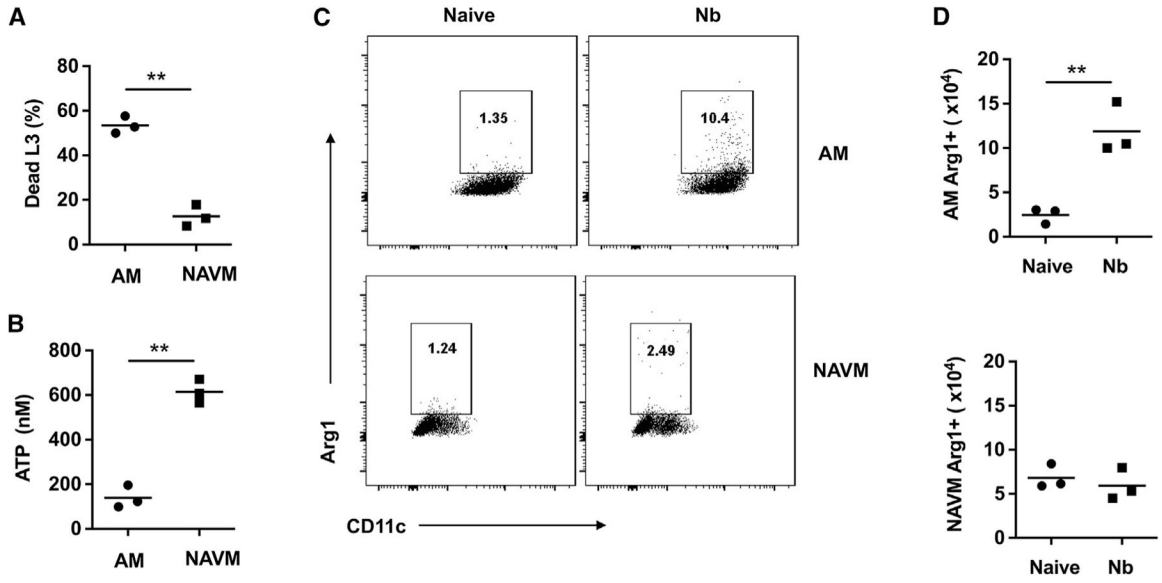

Figure 2. AMs preferentially contribute to parasite killing and express high arginase

(A and B) Lung AMs and NAVMs were stained as in Figure 1 and sort-purified from whole lung-cell suspensions at day 7 after *N. brasiliensis* inoculation of BALB/c mice. AMs and NAVMs were seeded to 24-well plates (1×10^6 cell/well) and co-cultured with 100 exsheathed third-stage larvae (L3). At day 5 after culture, the percent mortality (A) and worm ATP concentration (B) were determined. This experiment was repeated three times with similar results.

(C and D) Representative flow cytometry plots (C) and lung macrophage numbers (D) for cytoplasmic arginase protein expression in AMs and NAVMs at day 7 after *N. brasiliensis* inoculation.

Each symbol represents triplicates of pooled samples (A and B) or individual mice (D), and horizontal lines indicate the mean. All results are representative of two independent experiments. **$p < 0.01$(Student's t test).

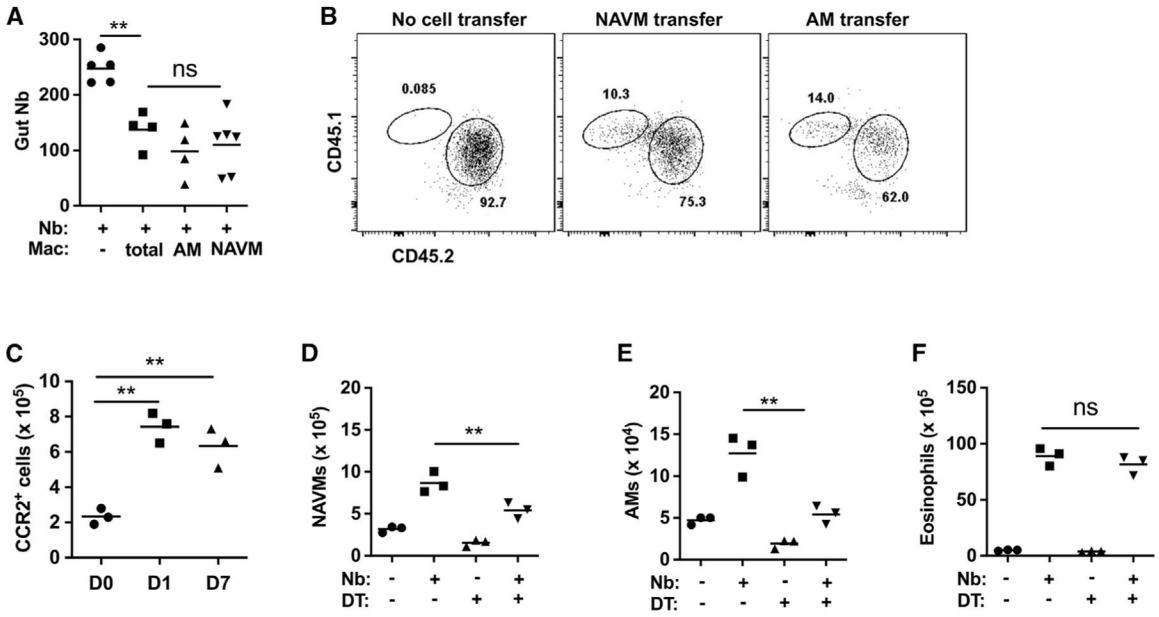

Figure 3. Lung-infiltrating monocytes acquire a tissue-resident phenotype and contribute to the increased AM population after *N. brasiliensis* inoculation

(A) At day 7 after *N. brasiliensis* (Nb) inoculation, donor macrophages including total macrophages, AMs, and NAVMs were electronically sorted and transferred to recipient mice, which were inoculated with Nb 2 days later. Recipient mice were assayed for intestinal worm numbers at day 5 after inoculation; a control group did not receive macrophages.

(B) Donor CD45.1 mice were inoculated with Nb, and 7 days later, lung NAVMs and AMs (as described in Figure 1) were sort-purified and transferred intratracheally (i.t.) into naive recipients (CD45.2), which were inoculated with Nb 2 days later. Donor and recipient lung AM populations were assessed at day 5 after Nb inoculation. Flow cytometry plots were representative of 3 mice per group and 2 independent experiments.

(C) CCR2-GFP reporter mice were assessed by flow cytometric analysis for monocyte recruitment to total lungs at days 1 and 7 after Nb inoculation.

(D–F) Monocytes were depleted by administration of DT at −1, +1, and +3 after Nb inoculation of CCR2-DTR mice. At day 7 after Nb inoculation, numbers of total lung NAVMs (D), AMs (E), and eosinophils (F) were determined by flow cytometric analysis. Each symbol represents an individual mouse, and horizontal lines indicate the mean. All results are representative of two independent experiments. **$p < 0.01$ (one-way ANOVA).

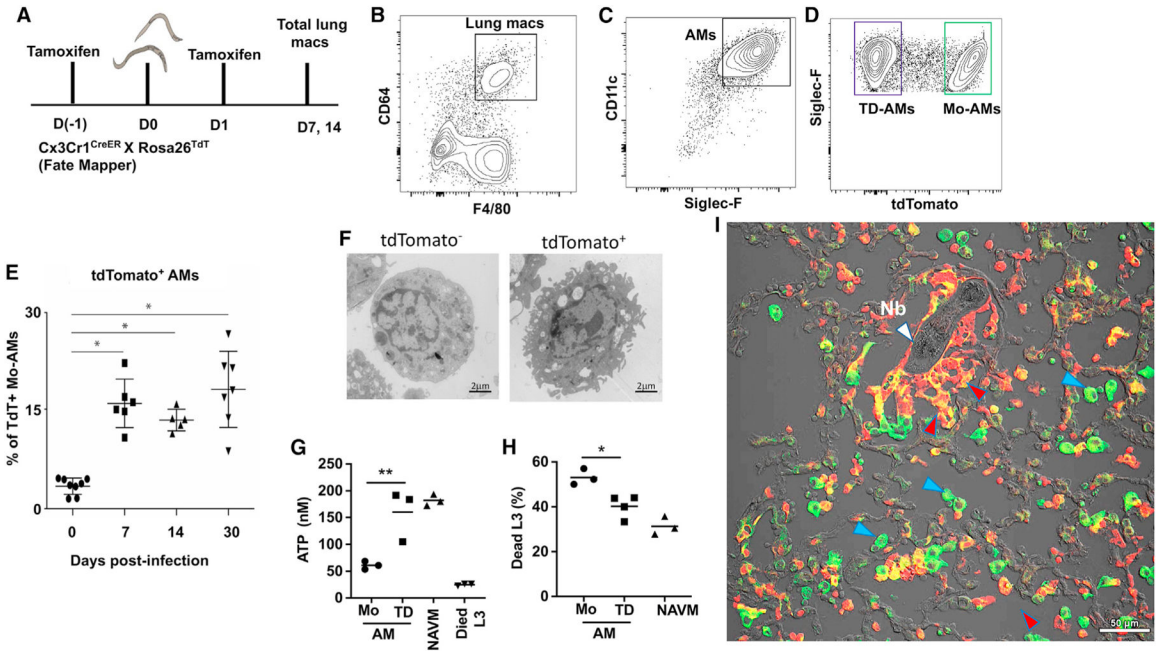

Figure 4. Monocyte-derived AMs preferentially damage and kill *N. brasiliensis* L3

(A–D) Fate-mapping of monocyte-derived macrophages recruited to the lung after Nb infection. Five mice were pulse-administered TAM at days −1 and +1 after Nb inoculation (Figure 4A). Whole lung was collected at days 7 and 14 after inoculation, and single cell suspensions were stained for AMs as described in Figure 1. F480^{+}, CD64^{+} lung macrophages were gated for expression of CD11c and SiglecF (B and C), and double-positive cells were in turn gated for tdTomato expression (D).

(E)Whole lung-cell suspensions from *Cx3*cr1$^{\text{CreERT2-IRES-YFP/+}}$Rosa26$^{\text{floxed-tdTomato/+}}$ reporter mice were assessed for tdTomato (tdT)$^{+}$ monocyte-derived AMs (Mo-AMs) at different timepoints after Nb inoculation. Each symbol represents individual mice, horizontal lines indicate the mean, and error bar represents SEM. *$p < 0.05$ (Student's t test).

(F)tdT^{-} and tdT^{+} cells were sort-purified on day 30 post-infection and prepared for ultrastructural analysis via TEM (magnification 3,800×; scale bar, 2 μm).

(G and H) Lung tdT^{+} (tdT^{+} AM) monocyte-derived AMs and tdT^{-} (tdT-AM) tissue-derived AMs were sort-purified from Nb-primed *Cx3*cr1$^{\text{CreERT2-IRES-YFP/+}}$Rosa26$^{\text{floxed-tdTomato/+}}$ reporter mice at day 7 post-infection. Macrophage subsets were seeded to 24-well plates (1×10^{6} cell/well) and co-cultured with 100 exsheathed L3. At day 5 after culture, worm ATP concentration (G) and percent mortality (H) were determined. Triplicate samples were assayed from pools of 20 larva from each well for determination of ATP concentration. Each symbol represents mean of triplicate samples, horizontal lines indicate the mean, and this experiment was repeated three times with similar results. *$p < 0.05$, **$p < 0.01$ (one-way ANOVA).

(I)Lungs from *Cx3*cr1$^{\text{CreERT2-IRES-YFP/+}}$Rosa26$^{\text{floxed-tdTomato/+}}$ reporter mice were collected after a second inoculation with Nb, sectioned, and stained with an APC-CD11c antibody for confocal immunofluorescence imaging analysis of CD11c and tdT expression. Image is representative of a total of 8 individual mice. White marker, Nb larvae; blue marker,

CD11c^{+}, tdTomato^{-} TD-AMs; and red marker, CD11c^{+}, tdTomato^{+} Mo-AMs. Scale bar, 50 μm.

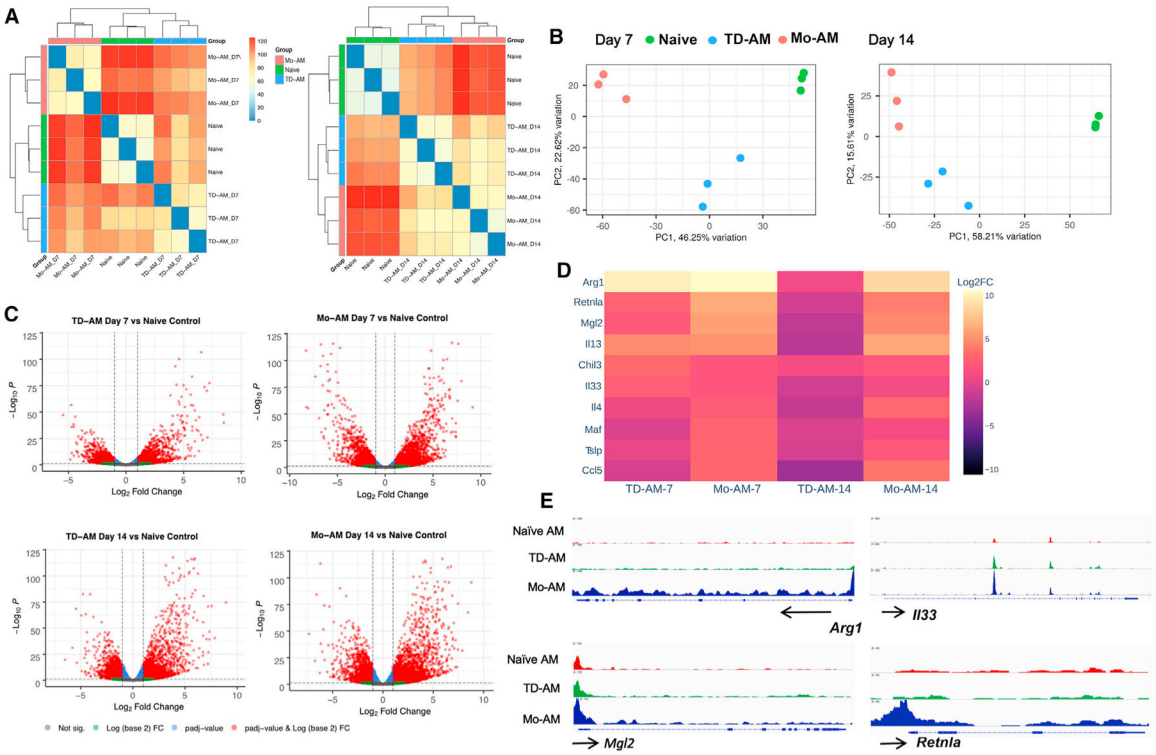

Figure 5. Mo-AMs have distinct phenotype characterized by upregulation of type 2 markers

(A–E) *Cx3*cr1$^{\text{CreERT2-IRES-YFP/+}}$Rosa26$^{\text{floxed-tdTomato/+}}$ reporter mice received TAM at days −1 and +1 after Nb infection. At days 7 and 14, tdT^{+} Mo-AMs and tdT^{-} tissue-derived AMs (TD-AMs) were sort-purified for RNA-seq transcriptional analysis and compared with naive AMs, with 3 mice/treatment group.

(A) Pairwise Euclidean distance relative to the transcriptional profiles, demonstrating sample relatedness between AMs from untreated mice, and Mo-AMs and TD-AMs at days 7 and 14 after Nb inoculation.

(B) Principal-component analysis of transcriptional profiles of treatment groups.

(C) Volcano plots of TD-AMs and Mo-AMs individual gene expression profiles at days 7 and 14 expressed relative to AMs from naive mice.

(D) Expression of selected characteristic type 2 response markers in TD-AMs and Mo-AMs at days 7 and 14 after Nb inoculation as expressed relative to AMs from naive mice ($\log_2$ fold change).

(E) Genome browser views of *Arg1*, *Il33*, *Mgl2*, and *Retnla* in naive AMs, TD-AMs, and Mo-AMs. Each track represents the normalized read counts of accessible chromatin regions. See also Figures S2 and S3

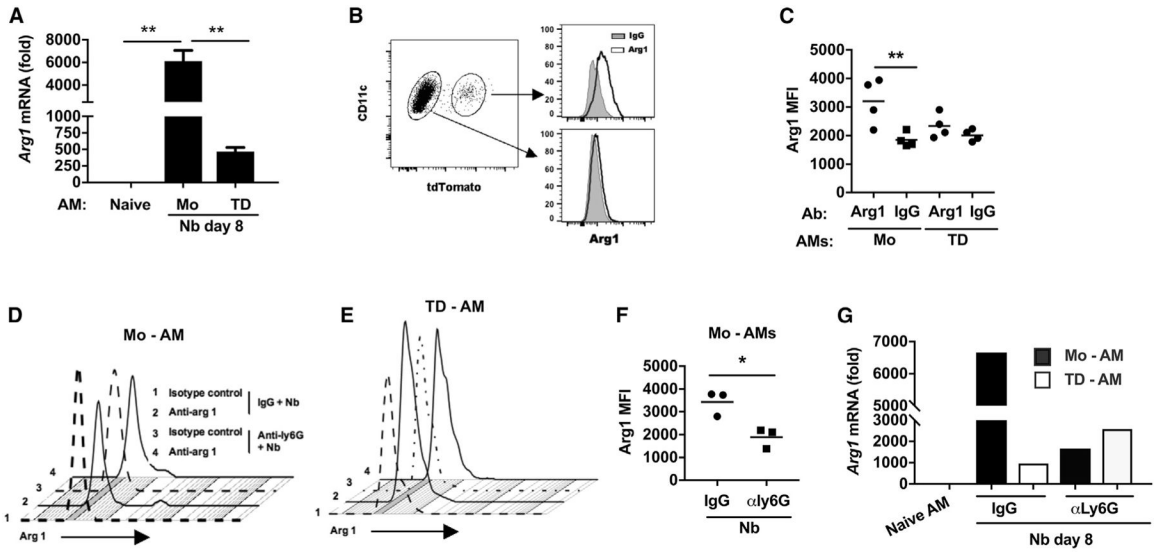

Figure 6. After *N. brasiliensis* infection, Mo-AMs preferentially express arginase 1, which is dependent on extrinsic neutrophil signaling

(A–C) *Cx3*cr1$^{\text{CreERT2-IRES-YFP/+}}$Rosa26$^{\text{floxed-tdTomato/+}}$ reporter mice were administered TAM and inoculated with Nb as described in Figure 5.

(A) Arginase 1 (Arg1) mRNA levels by qPCR in subpopulations of lung AM subsets at day 8 after Nb inoculation expressed relative to naive AMs.

(B and C) Representative flow cytometric analysis of Arg1 intracellular protein expression in AM subsets at day 7 after Nb inoculation (B) and (C) Arg1 mean fluorescence intensity (MFI) in individual samples from different treatment groups (C).

(D–G) *Cx3*cr1$^{\text{CreERT2-IRES-YFP/+}}$Rosa26$^{\text{floxed-tdTomato/+}}$ reporter mice were administered anti-Ly6G Ab or isotype control at days −1, 1, and 3 and given TAM at days −1 and +1 after Nb inoculation.

(D and E) Representative flow cytometric analyses of Arg1 intracellular protein expression after neutrophil depletion.

(F) Arg1 MFI in individual samples from each treatment group. Each symbol represents an individual mouse, and horizontal lines indicate the mean.

(G) Arg1 mRNA levels by qPCR in macrophage subsets, presented as the fold increase over naive AMs.

Data shown are the mean and SEM of triplicate samples (A) or pooled samples (G) from a total pool of four to eight mice per group. All results are representative of at least two independent experiments. *$p < 0.05$, **$p < 0.01$ (one-way ANOVA).

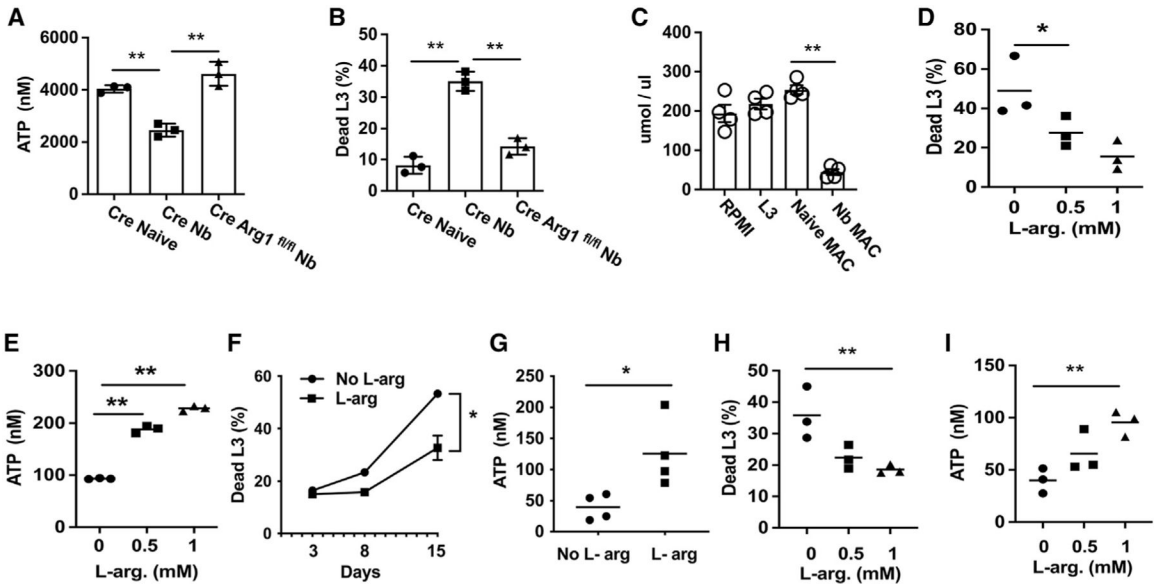

Figure 7. L-arginine depletion by Nb-activated lung macrophages kills parasitic larvae

(A and B) Tie2-Cre (CRE) and Tie2-Cre Arg1$^{fl/fl}$ (Cre Arg1$^{fl/fl}$) mice were inoculated with Nb L3, and 7 days later, total lung macrophages were sort-purified and cultured (1×10^6 cells/well) for 5 days with 100 Nb exsheathed L3 and assayed for worm ATP (A) and percentage of mortality (B).

(C) Arginine levels in supernatant were measured in cultures with L3 or co-cultures with sort-purified naive lung macrophages or lung macrophages isolated from Nb at day 5 after culture.

(D and E) Sort-purified total lung macrophages from Nb-inoculated mice were co-cultured with Nb exsheathed L3 naive macrophages and supplemented with L-arginine. At day 5 after culture, the percentage of mortality (D) and larval ATP concentration (E) were determined, as described in Figure 4.

(F and G) Exsheathed Nb larva (100 L3) were seeded to 12-well plates and cultured with L-arginine-free RPMI 1640 media, with one group supplemented with L-arginine. At days 3, 8, and 15 after culture, the percentage of mortality was assessed (F), and the remaining worm ATP concentration assessed at day 15 (G).

(H and I) Total lung macrophages were sort-purified from Nb-inoculated mice as described above and co-cultured with *H. polygyrus* L3. Percentage of mortality (H) and worm ATP concentration (I) were assessed.

Data are presented as the mean and SEM of triplicate samples (F) or as individual samples obtained from 20 larva from each well for the determination of the percentage of mortality, and ATP concentration and horizontal lines indicate the mean (A–E and G–I). All results are representative of at least two independent experiments. *$p < 0.05$, **$p < 0.01$ (one-way ANOVA, A–E, H, and I; Student's t test, F and G).

KEY RESOURCES TABLE

REAGENT or RESOURCE	SOURCE	IDENTIFIER
Antibodies		
Rat IgG2a isotype control (clone 2A3)	BioXcell Cat# BE0089	RRID: AB_1107769
Anti-Ly6G (1A8),	BioXcell Cat#BE0075-1	RRID: AB_1107721
Anti-CD11b,	BD Bioscience CaT#563553	RRID: AB_2738276
Anti-CD11c,	BD Bioscience Cat#564080	RRID: AB_2738580
Anti-CD11c	BD Bioscience Cat#565452	RRID: AB_2744278
Anti-Siglec F,	BD Bioscience Cat# 562681	RRID: AB_2722581
Anti-SiglecF,	BD Bioscience Cat#565526	RRID: AB_2739281
Anti-F4/80,	Biolegend Cat# 123116	RRID: AB_893481
Anti-CD64	Biolegend cat#139314	RRID: AB_2563904
Anti-CD45	Biolegend cat#103149	RRID: AB_2564590
Anti-CD45.1	eBioscience cat#11-0453-81	RRID: AB_465058
Anti-CD45.1	Biolegend cat#110715	RRID: AB_313504
Anti-CD45.2	Biolegend cat#109823	RRID: AB_830788
Anti-Ly6C	eBioscience cat#12-5932-81	RRID: AB_10804510
Anti-Ly6C	eBioscience cat#53-5932-82	RRID: AB_2574427
Anti-Ly6C	eBioscience cat#45-5932-82	RRID: AB_2723343
Anti-Arg1	R&D systems cat#5868A	RRID: AB_2810265
Anti-Arg1	R&D systems cat#5868P	N/A
Anti-IL-13	eBioscience cat#12-7133-82	RRID: AB_763559
Chemicals, peptides, and recombinant proteins		
Liberase™	Roche cat#5401127001	N/A
Tamoxifen	Sigma-Aldrich cat#T5648	N/A
Diphtheria Toxin	Sigma-Aldrich cat#D0564	N/A
Critical commercial assays		
Click-iT Plus EdU Flow Cytometry Assay Kits	Thermofisher cat#C10634	N/A
Arginine Assay Kit (Fluorometric)	Abcam cat#ab252892	N/A

REAGENT or RESOURCE	SOURCE	IDENTIFIER
Experimental models: Organisms/strains		
N. brasiliensis	This paper	N/A
H. polygyrus	This paper	N/A
WT BALB/c	Jackson Laboratory	JAX:000651
WT BL/6	Jackson Laboratory	JAX:000664
BALB/c ByJ (CD45.1),	Jackson Laboratory	JAX:006584
Rosa26floxed-tdTomato	Jackson Laboratory	JAX: 007909
Cx3cr1CreERT2-IRES-YFP	Jackson Laboratory	JAX: 020940
Il4ra/BALB/c	Jackson Laboratory	JAX:003514
Tie 2-Cre and Tie2-Cre Argfl/fl mice	Dr. Peter J. Murray	Max Planck Institute of Biochemistry, Martinsried 82152, Germany.
CCR2-DTR, CCR2-GFP mice	Dr. Amariliz Rivera	Department of Pediatrics, New Jersey Medical School, Rutgers—The State University of New Jersey, Newark, New Jersey, USA
Oligonucleotides		
PCR primer for arginase 1	Thermo Scientific	Mm00475988_m1
Software and algorithms		
Statistical software program Prism	GraphPad Software	https://www.graphpad.com/
Other		
RNA-seq	This paper	GSE189675
ATAC-seq	This paper	GSE189674